POLITECNICO DI TORINO

Master of Science in Biomedical Engineering - Biomedical Instrumentation

Master's Degree Thesis

Finite element model of transport phenomena through nanofluidic system for medical applications

Supervisors

Prof. Danilo DEMARCHI

Prof. Alessandro GRATTONI

Nicola DI TRANI

Candidate

Nevio RACCA

March 2021

"Istruitevi, perché avremo bisogno di tutta la nostra intelligenza.
Agitatevi, perché avremo bisogno di tutto il nostro entusiasmo.
Organizzatevi, perché avremo bisogno di tutta la nostra forza."
Antonio Gramsci

Abstract

Micro and nanofluidic phenomena represent an increasing interest area in research community. The high surface-volume ratio has shown fluidic behavior that differs from the bulk and finds applications in many different fields, from energy harvesting to medical devices. The widespread adoption and investigation of micro-nanofluidic technologies is mainly thank to the advancement in micro and nano fabrication techniques.

Specifically, the use of nanofluidic membranes has shown incredible effectiveness in drug delivery applications. They allow zero-order drug release kinetics thanks to molecular nanoconfinement, where the nanochannels size represents the limiting factor for drug diffusion. Moreover, the implementation of an electrically gated Bio-FET structure in the nanochannels can be used to control the release kinetics of charged molecules in solution offering a promising technique for controlled drug delivery.

Extensive experimental analyses are needed to correctly optimize these nanofluidic systems for their specific application, which can result in considerable time and money expenditure. *In silico* simulations through finite element methods (FEMs) analysis represents a relatively inexpensive strategy for the first steps of device optimization leading to a faster and cheaper product development. A properly designed and validated model, can help device development by simulating hundreds or thousands of possible scenarios, which would be unfeasible to experimentally realize, not to mention that it would require a prohibitive amount of money.

Although, several FE models have been developed to simulate electrically gated nanochannel, all diluted molecules are considered as point-like. Especially in medical applications, used drugs may have a dimension comparable to the nanochannel size, therefore it cannot be neglected.

Here, in collaboration with Dr. Alessandro Grattoni Laboratory at the Houston Methodist Research Institute, I have developed a finite element model to simulate the concentration driven diffusion of charged particles in electrostatically gated nanofluidic membranes for drug delivery.

To overcome the previously mentioned problems, the bi-dimensional finite element model developed includes the most realistic features present in previous models with the addiction of not negligible sizes for diluted ions. The equations used to account for particles sizes are inspired from previously developed numerical models that, however, do not consider a bi-dimensional geometry. A single dimension model is also developed in tandem, to validate the results obtained with previous numerical models.

The effects of several parameters such as drug and nanochannel dimensions and ionic strength of the solution, just to name a few, are independently studied to better characterize their influence on solute enrichment or depletion in nanoconfinement.

The obtained results show interesting and not negligible differences from classical FE models where particle sizes are neglected. To further validate the model, the results obtained are compared with experimental data obtained from the laboratory of Dr. Grattoni, showing a good agreement. Additionally, results obtained with the bi-dimensional model have shown improved fitting to experimental data, when compared to 1D FEM models.

Table of Contents

List of Tables VII

List of Figures VIII

I Introduction and FEM description 1

1 Introduction 2
- 1.1 About FEMs and nanochannels . . . 2
- 1.2 Current approaches . . . 8
- 1.3 Equations . . . 10

2 FEM description 16
- 2.1 Model description . . . 16
- 2.2 Geometry and materials . . . 18
- 2.3 Physics . . . 20
- 2.4 Boundary conditions . . . 21

II Results and discussion 25

3 Model validation 26
- 3.1 Surface charge density . . . 26
- 3.2 Modified PNP . . . 31

4 Model results 34
- 4.1 Membrane properties effects on V_{surf} . . . 34
- 4.2 Membrane properties effects on EEF . . . 39
- 4.3 Drug properties effects on EEF . . . 46

5 Comparison with experimental data 53
5.1 Introduction 53
5.2 FEM application 55

6 Conclusion 60

Bibliography 62

List of Tables

1.1 Debye's lengths 4

2.1 Boundary conditions in 1D model 21
2.2 Bulk concentration values for 1D study 22
2.3 Boundary conditions in 2D model 23
2.4 Bulk concentration values for 2D study 24

List of Figures

1.1 EDL structure 6
1.2 Example of Bio-Fet 6
1.3 Dr Grattoni's membrane 7
1.4 Modified PNP equation effects 11

2.1 2D geometry from COMSOL model 19

3.1 Surface charge density validation with Pardon - Part 1 26
3.2 Surface charge density validation with Taghipoor 27
3.3 Surface charge density validation with Pardon - Part 2 28
3.4 Final model surface charge density validation 29
3.5 Donnan equilibrium 31
3.6 Drug molecules saturation 32

4.1 Binding sites density effects on V_{surf} 35
4.2 Dielectric material properties effects on V_{surf} 36
4.3 Interaction between V_{gate} and σ 37
4.4 Surface potential effects on EEF 39
4.5 Channel dimension effects on EEF - Solution ionic strength influence 42
4.6 Channel dimension effects on EEF - V_{surf} influence 43
4.7 Channel dimension effects on EEF - Stern layer capacitance influence 45
4.8 Counter-ions saturation due to drug size 47
4.9 Counter-ions EEF saturation due to drug-salt ratio - Drug valence . 48
4.10 Counter-ions EEF saturation due to drug-salt ratio - Drug bulk concentration 49
4.11 Maximum drug concentrations 50
4.12 Co-ions EEF saturation due to drug-salt ratio - Drug valence 51
4.13 Co-ions EEF saturation due to drug-salt ratio - Drug bulk concentration 52

5.1 Experimental results of nanofluidic membrane 54
5.2 FE model reproduction of experimental results 59

Part I

Introduction and FEM description

Chapter 1

Introduction

1.1 About FEMs and nanochannels

Finite element methods can be really useful to understand phenomena at very low dimensional scale, as micrometric, nanometric and ultra-nanometric scale [1]. At such scales it is quite impossible to use measurement tools during experimental tests, but, using a FEM software a direct measurement of specific parameter becomes possible, reducing costs and saving time [2, p. 84]. They cannot substitute experimental tests, but they can provide a useful acknowledgement on physical phenomena involved and optimize environmental conditions performing thousands of simulations on several parameters.

This thesis is focused on the behavior of charged particles diluted in a solution passing through a nanochannel.
Physical phenomena that are usually neglected at macroscopic scale can assume a relevant role at nanofluidic scale where surface effects dominate against volume forces [3, 4, 5, 6]. Especially, electric phenomena, whose effect is usually inversely proportional to distance from the electric charge, have a main role at nanometric distances.
Indeed, in a nanofluidic channel, where a solution with charged ions diluted is in contact with a solid wall, chemical reactions at the solid-liquid interface show a net charge and an electric potential, consequently. This potential, or an externally applied one, leads to an enrichment next to the wall of ions with an opposite charge (counter-ions) respect to that one of wall and a depletion of those with same one (co-ions) [7]. In this way the opposite-sign charges diluted inside the solution screen the potential at the solid surface to maintain the electroneutrality [8].

This phenomenon is called electric double layer (EDL) and its structure is shown

in figure 1.1. There are several theories about its real composition. In this paper the Guy-Chapman-Stern theory is used to model it [9]. Basically, the EDL is here considered as composed by the diffusive plane and the Stern layer, without any distinction between inner and outer Helmholtz planes.
Stern layer is generally considered as the first layer of adsorbed ions at the solid surface.

Considering its effect on a nanofluidic channel where charged molecules diffuse from a high concentration location to an empty one, the concentration of counter-ions and co-ions is locally increased and decreased next to charged walls, respectively. The length of EDL compared with nanochannel width is indicative of effective importance of this phenomenon on total diffusive flux of the charged drug. EDL length is at the same magnitude order of Debye's length expressed in equation 1.1 [9].

$$\lambda_D = \left(\frac{e^2 \sum_i n_i^\infty z_i^2}{\epsilon_0 \epsilon_r k_B T} \right)^{-\frac{1}{2}} \tag{1.1}$$

In eq. 1.1, e is the elemental charge, $n_i^\infty = 1000 N_A c_i$ is the bulk volume density of i-ions (N_A and c_i are the Avogadro's number and the molar concentration of i-ionic species, respectively), z_i is the valence of i-ionic species, ϵ_0 and ϵ_r are the absolute and relative permittivity, respectively, k_B is the Boltzmann's constant and T is the temperature expressed in Kelvin. As described by this equation, Debye's length is inversely proportional to ions concentrations, because with a higher amount of electrolytes diluted in the solution the electric potential at the solid surface is more easily screened leading to a shorter EDL. On table 1.1 it is possible to see which order of magnitude the Debye's length assumes at different diluted salt concentrations, which is considered as the main ionic species that influences ionic strength of the solution. The latter term is proportional to the total amount of diluted ions within a solution, both positive and negative species. It is equal to $\frac{1}{2} \sum c_i z_i^2$ and c_i and z_i are concentration and valence of i-ion, respectively.

Active implantable devices for controlled drug release can use EDL effects for their task. Indeed, using a membrane with sufficiently narrow channels between the inner reservoir of device and patient body environment and applying an external electric potential, the channels walls should assume a specific potential that influences the distributions of co-ions and counter-ions and their fluxes. Then, using a drug that assumes a non-zero charge in physiological environment, the flux of this molecule can be increased or decreased, at even stopped, respectively applying at the membrane an opposite or same-sign voltage.

KCl concentration (M)	**Debye length λ_D (nm)**
1	0.3
0^{-1}	1
10^{-2}	3.1
10^{-3}	9.6
10^{-4}	30.5
10^{-5}	96.3

Table 1.1: Debye's lengths with different salt ions concentrations [9]

The realistic reproduction of nanofluidic phenomena with a finite element software is an interesting and even more studied field since many years [1]. Indeed, governing equations that solve the coupling of concentration of charged drug and the electric potential distribution in a electrolytes solution, Nernst-Planck and Poisson, respectively, can be solved analytically only with really restrictive conditions. But they can be solved numerically overcoming these restrictions [7].
Due to those advantages, different FE models had been developed. Obviously, different tasks were focused by previous models. One of the most commonly studied case of these applications is the Bio-FET. Its structure is shown in figure 1.2. This specific geometry is mainly composed by two differently applied electric fields. The first one is the drain-source voltage, axially applied to the nanochannel, and the second one is the gate potential, which is usually referred to a common ground with previous voltage and applied at the gate electrode. The last electric field is normal to nanochannel axial direction.
Combining these two voltages it is possible to control the fluxes of ionic species through the channel in different ways. The axial electric field causes an electrophoretic flux of ions axially to the channel. Instead, the gate voltage or a natural charge of solid material in contact with the solution causes the EDL structure previously explained [9]. Other phenomena, as the electroosmotic flux, are involved in these applications, but they are not explained due to the negligible relevance in this thesis.

The purposes of this thesis are the reproduction and the explanation of experimental results obtained by the nanoporous membrane developed by Dr. Grattoni and Di Trani at Houston Methodist Research Institute for controlled drug release application. The figure 1.3 shows its general structure and fabrication process. The mean diameter of channels in this device is 300 nm. 60 nm is the thickness of deposited silicon carbide layer over the Poly-Silicon one which is used as buried gate electrode [10]. A not ideal deposition of dielectric layer is hypothesized, assuming that the 60nm-thick layer, due to the high porosity of the used material [11], should be realistically simulated with a thinner layer. This assumption is tested in this

thesis.
For this reason, differently from most of literature cases, the FEM shown in this thesis has the task to reproduce the diffusion of a charged drug through an electrostatically gated nanochannel. The all thesis will focus on this specific application, without considering the complete Bio-FET structure, as the presence of a drain-source voltage, because the proposed nanochannel structure is developed for a biomedical engineering application for an active implantable device, so the power consumption is extremely important [10].

To evaluate the effect of EDL on drug flux, an indicative parameter will be used: the exclusion/enrichment factor (EEF or β) [12]. This parameter is calculated as the ratio between the effective mean concentration of drug inside the nanochannel and its concentration if it was a neutral molecule and only a diffusive flux takes place through the channel, as shown in equation 1.2 [9].
EEF is assumed as equal to the ratio between effective permeability of channel on a probe molecule and its normal permeability, when no electrical voltage is externally applied and the movement of ions inside channel is unaffected [13]. This assumption is tested and verified in this thesis.

$$\beta = \frac{C_{eff,D}}{C_{b,D}} = \frac{\bar{C}_D}{C_{b,D}} \tag{1.2}$$

$C_{eff,D}$ is the effective concentration of drug and $C_{b,D}$ the bulk drug concentration. It represents the concentration of charged molecules where the electric potential is zero, usually in the middle of nanochannel. In this case, it means the concentration not affected by an electric field.
As it is usually done in literature, the effective concentration, is calculated by the arithmetic mean of each value in the nanochannel ($\bar{C}_D$)[14].
A $\beta > 1$ means that the drug is an enriched counter-ion and its mean concentration is higher than the bulk value. $\beta < 1$ is the consequence of the exclusion of drug from channel because it is a co-ion.

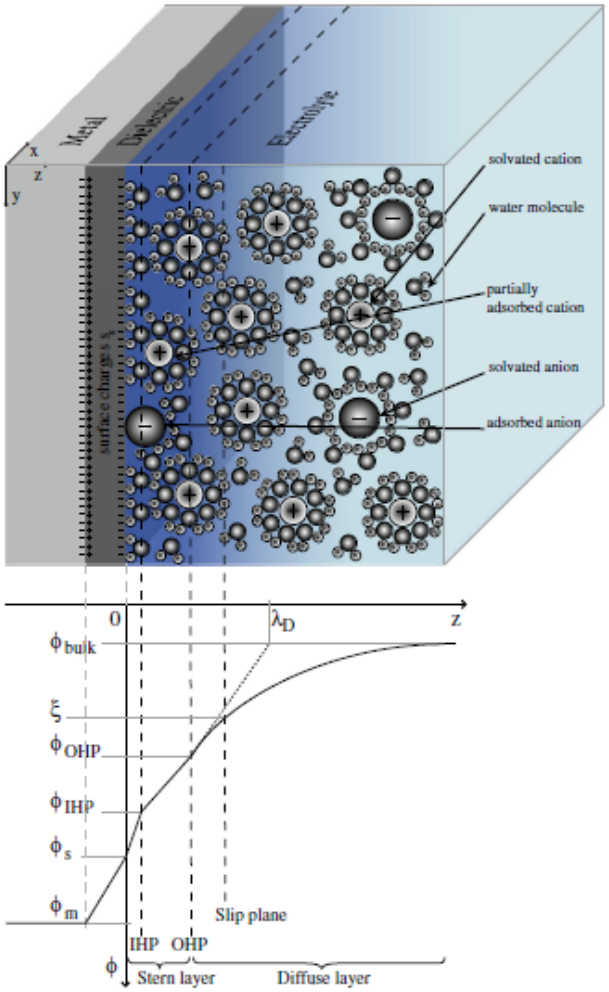

Figure 1.1: EDL structure [7]

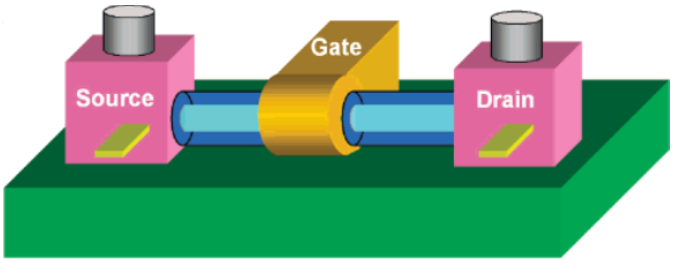

Figure 1.2: Example of Bio-Fet [8]

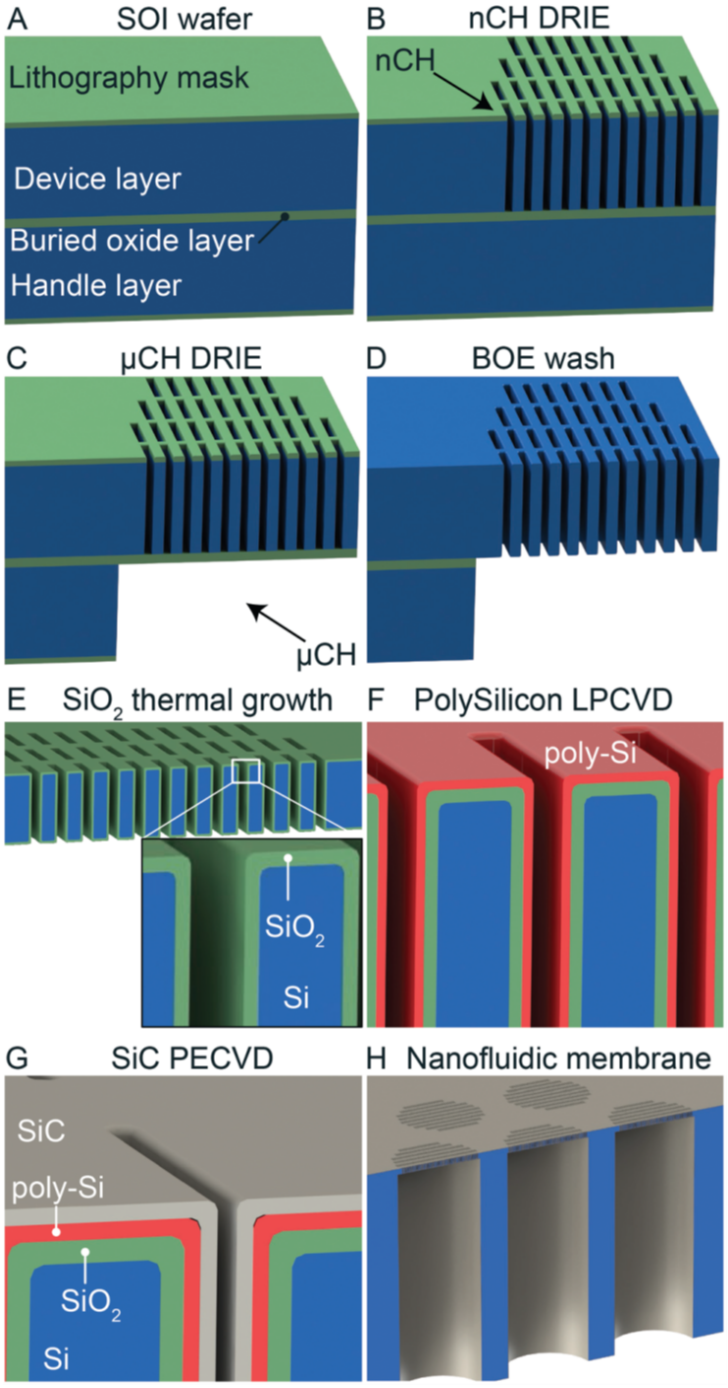

Figure 1.3: Membrane developed by Di Trani and its manufacturing process. Fabrication process schematics: A) Silicon on insulator (SOI) wafer with lithography mask B) deep reactive ion etching (DRIE) for nanochannel (nCH) patterning. C) DRIE for microchannel (CH) pattern. D) SiO2 mask removal. E) SiO2 thermal oxidation growth. F) Conductive poly-Si deposition. G) Insulating SiC deposition. H) Membrane structure [10]

1.2 Current approaches

A literature research was previously done to evaluate the actually present finite element models that already exist and if it was reasonable the need of developing a new one

Pardon's model does not specifically study these phenomena in a drug delivery application [7]. His study focuses on background analytes concentrations (as salt ions) and their fluxes caused by an electrophoretic force inside a Bio-FET as in figure 1.2. Due to this different task in this model, the specific diffusion of a charged and finite-size particles is not studied, but the influence of EDL on ions movement through gated channel due to the axial electric field generated by a drain-source voltage is done. Even if the focus of his model is different, other phenomena he has considered, such as the Multisite Complexation (MUSIC) model, which is used to simulate the surface charge density at solid-liquid interface, are developed in this thesis model as well. But in an active implantable device application, power consumption represents a main problem and for this reason a study on the unique effects of voltage gate on the diffusive flux of a charged drug is needed.

Eden has published a study with a similar model that focus on diffusion of a charged sample species. But, differently from Pardon, he used a fixed surface charge density, which limits the use of his model to experimentally measured value in specific conditions. Furthermore, a drain-source voltage is still considered in his study [15].

Kim has presented a model that, inspired by Pardon, studies the diffusion movement of a charged particle modulated only by a voltage gate applied at channel walls. He also uses a MUSIC model to simulate the surface charge density value [13, 16]. His model is the most similar FE one developed with COMSOL software to this thesis work, which differs from latter model on the different consideration of diluted molecules.

Indeed, all the previous models do not consider the drug size as relevant on its flux. They all assume its size does not affect EDL length. This assumption is overcome in my model which, using a modified diffusion module that considers the finite size of each ions diluted in the solution, correctly models the influence of ions size on diffusive fluxes and their concentrations in the channel. The relevance of drug size is studied in different environmental conditions in this thesis.

Therefore, the finite element model proposed in this work can realistically simulate the diffusion of studied charged drug from the high concentrated reservoir

to the outside of the medical device. The model can simulate the surface charge density at solid-liquid interface that changes accordingly with ions concentrations and the ions diffusion through the channel with an externally applied gate potential. Thanks to the developed model, an unrealistic enrichment of counter-ions next to the channel wall is avoided, because the software rightly simulates the achieving of the maximum packaging concentration for each drug size.

1.3 Equations

1.3.1 Poisson-Nernst-Planck equations

As aforementioned, FE models overpass the restrictions of analytical solvers due to their numerical computation. Indeed, the behavior studied in this thesis, the diffusion of charged ions inside an electrolytes solution is described by the coupling of two different equations: Poisson and Nernst-Planck (NP).
These two equations, shown in eq. 1.3 and 1.4, respectively, influence each others and are coupled together [7]. Indeed, Poisson equation defines the electric potential inside the solution as dependant on the concentrations of diluted ions. On the other hand, Nernst-Planck equation defines the concentrations of each ionic species based on electric potential in the solution. Nernst-Planck equation describes also the movements of diluted ions due to concentration gradients, fluid fluxes or chemical reactions that take place inside the solution.

$$\nabla^2\phi = -\frac{\rho_{el}}{\epsilon_0\epsilon_r} \tag{1.3}$$

$$\frac{\partial c_i}{\partial t} + \nabla(c_i\boldsymbol{u}) - \nabla(D_i\nabla c_i + z_i\mu_{m,i}Fc_i\phi) = R_{chem,i} \tag{1.4}$$

In eq. 1.3 ρ_{el} is the space charge density inside the solution equal to $10^3 N_A \sum_i ec_i z_i$. In the equations above, these are the variables: ϕ is the electric potential, ϵ_0 and ϵ_r are the absolute and relative permittivity, respectively, e is the elemental charge, N_A the Avogadro's number, c_i the molar concentration of i-ion, z_i the valence of i-ion, $\boldsymbol{u}$ the fluid velocity, D_i the diffusion coefficient of i-ion, $\mu_{m,i}$ the mobility of i-ion, F the Faraday's constant and $R_{chem,i}$ the term accounting production or consumption rates from chemical reactions.
In the following equations 10^3 term is usually used to convert concentration values expressed in M unit to mol/m^3 because the other dimensional parameters are expressed with m^3 unit, not L.
Solving these two equations at the chemical equilibrium ($R_{chem,i} = 0\ \frac{mol}{m^3 s}$), without any fluid flow ($\boldsymbol{u} = 0\ \frac{m}{s}$) and at steady state condition ($\frac{\partial c_i}{\partial t} = 0\ \frac{M}{s}$), the Poisson-Boltzmann equation is obtained (equation 1.5).

$$\nabla^2\phi = -\frac{10^3 N_A e}{\epsilon_0\epsilon_r}\sum_i c_{0,i} z_i \exp\frac{-z_i e\phi(z)}{k_B T} \tag{1.5}$$

$\mu_{m,i}$ is derived from Einstein's relation and it is equal to D_i/RT. Due to the fact that, in literature, concentration variables are expressed with $1/m^3$ unit and not with M, different versions of Einstein's relation could be found. This one is adapted to molar concentrations. $c_{0,i}$ is the bulk concentration (also addressed as c_i^b). The

potential is dependant on z which is the normal direction from channel wall. In this case only an electric potential applied to the wall is considered which means that it varies only changing distance from wall, not the axial position along the channel.
Using equation 1.5 and definition of ρ_{el} it is possible to explicit the c_i Boltzmann distribution as:

$$c_i = c_{0,i} \exp \frac{-z_i e \phi(z)}{k_B T} \tag{1.6}$$

1.3.2 Modified Poisson-Nernst-Planck equations

Equation 1.6 defines the distribution of i-ion as exponentially dependant on electric potential, without considering ions sizes. Indeed, when the molecules radius becomes not negligible, the theoretic concentration calculated from eq. 1.6 could exceed the maximum concentration of specific ion defined as $\frac{1}{10^3 v_{ion} N_A}\ M$, where $v_{ion} = d_{ion}^3$ and d_{ion} is the ionic diameter. In this paper the ions are considered not spherical but with a cubic shape to underestimate the maximum concentration.
A simply modified Boltzmann distribution was used by Nicola Di Trani in a different numerical model [14]. His equation was used to obtain a more realistic functioning. It is shown in equation 1.7.

$$c_i(z) = c_i^b \frac{\exp \frac{-z_i e \phi(z)}{k_B T}}{1 + \sum_j^M 10^3 v_j N_A c_j^b (\exp \frac{-z_j e \phi(z)}{k_B T} - 1)} \tag{1.7}$$

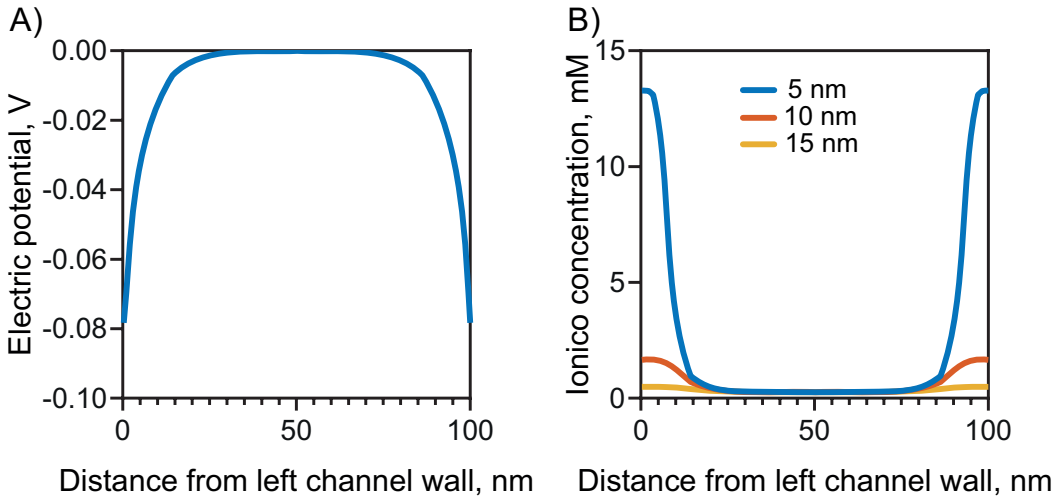

Figure 1.4: Example of modified PNP equation in a 100 nm width channel. **A**) Electric potential inside the channel. **B**) Result of eq. 1.7 calculated for a counter-ion with different ionic diameters

M is the number of ionic species with a not negligible radius. Using this distribution, ionic diameter becomes as more important as the potential ϕ is higher. Indeed, if a counter-ion has a relevant diameter, its concentration next to the charged wall saturates once reached its maximum concentration. It is possible to evaluate the effect of equation 1.7 for counter-ions distribution in figure 1.4.B. Here the equation above is calculated for a counter-ion molecule at different ionic diameters using the electric potential distribution that is shown in figure 1.4.A. The equation 1.7, once the maximum concentration is reached for each ionic diameter, maintains it as constant, avoiding an unrealistic higher enrichment. Indeed, maximum concentration are 13.28 mM, 1.66 mM and 0.49 mM for 5 nm, 10 nm and 15 nm as ionic diameter, respectively.

This modified Boltzmann distribution can be obtained as solution of Nernst-Planck equation if specific terms are changed. All the passages are described below starting from eq. 1.4 at steady state condition:

$$D_i \nabla c_i + z_i \mu_{m,i} F c_i \nabla \phi = 0$$
$$\nabla c_i = -\frac{z_i e}{k_B T} c_i \nabla \phi$$

∇c_i and $\nabla \phi$ are substituted with $\frac{dc_i}{dz}$ and $\frac{d\phi}{dz}$,respectively, because z is the only dimension where both variables change along. So, reducing dz at both terms:

$$\frac{dc_i}{d\phi} = -\frac{z_i e}{k_B T} c_i(\phi)$$

Boltzmann distribution of c_i is the solution to this equation, but, if a modified Nernst-Planck equation is wanted to be obtained, the last equation has to be modified to:

$$\frac{dc_i}{d\phi} = \frac{d}{d\phi}\left(c_i^b \frac{\exp \frac{-z_i e\phi(z)}{k_B T}}{1 + \sum_j^M 10^3 v_j N_A c_j^b (\exp \frac{-z_j e\phi(z)}{k_B T} - 1)} \right) =$$
$$= c_i^b \left(\frac{\frac{-z_i e}{k_B T} \exp \frac{-z_i e\phi(z)}{k_B T} (1 + \sum_j^M 10^3 v_j N_A c_j^b (\exp \frac{-z_j e\phi(z)}{k_B T} - 1))}{(1 + \sum_j^M 10^3 v_j N_A c_j^b (\exp \frac{-z_j e\phi(z)}{k_B T} - 1))^2} + \right.$$
$$\left. - \frac{\exp \frac{-z_i e\phi(z)}{k_B T} (1 + \sum_j^M 10^3 v_j N_A c_j^b (\exp \frac{-z_j e\phi(z)}{k_B T} - 1))'}{(1 + \sum_j^M 10^3 v_j N_A c_j^b (\exp \frac{-z_j e\phi(z)}{k_B T} - 1))^2} \right)$$

Multiplying both terms for $\frac{d\phi}{dz}$:

$$\nabla c_i + c_i^b \exp\frac{-z_i e\phi(z)}{k_B T}\left(\frac{\frac{z_i e}{k_B T}}{1+\sum_j^M 10^3 v_j N_A c_j^b(\exp\frac{-z_j e\phi(z)}{k_B T}-1)}+\right.$$
$$\left.+\frac{(1+\sum_j^M 10^3 v_j N_A c_j^b(\exp\frac{-z_j e\phi(z)}{k_B T}-1))'}{(1+\sum_j^M 10^3 v_j N_A c_j^b(\exp\frac{-z_j e\phi(z)}{k_B T}-1))^2}\right)\nabla\phi = 0$$
$$\nabla c_i + c_i^b \frac{\frac{z_i e}{k_B T}\exp\frac{-z_i e\phi(z)}{k_B T}}{1+\sum_j^M 10^3 v_j N_A c_j^b(\exp\frac{-z_j e\phi(z)}{k_B T}-1)} *$$
$$*\left(1+\frac{(1+\sum_j^M 10^3 v_j N_A c_j^b(\exp\frac{-z_j e\phi(z)}{k_B T}-1))'}{\frac{z_i e}{k_B T}(1+\sum_j^M 10^3 v_j N_A c_j^b(\exp\frac{-z_j e\phi(z)}{k_B T}-1))}\right)\nabla\phi = 0$$

Multiplying for D_i, using Einstein relation, considering $F = N_A e$ and $R = N_A k_B$ and substituting with eq. 1.7:

$$D_i\nabla c_i + z_i\mu_{m,i}Fc_i\left(1+\frac{(1+\sum_j^M 10^3 v_j N_A c_j^b(\exp\frac{-z_j e\phi(z)}{k_B T}-1))'}{\frac{z_i e}{k_B T}(1+\sum_j^M 10^3 v_j N_A c_j^b(\exp\frac{-z_j e\phi(z)}{k_B T}-1))}\right)\nabla\phi = 0$$

Solving the derivation on ϕ:

$$\left(1+\sum_j^M 10^3 v_j N_A c_j^b(\exp\frac{-z_j e\phi(z)}{k_B T}-1)\right)' = -\frac{e}{k_B T}\sum_j^M 10^3 z_j v_j N_A c_j^b \exp\frac{-z_j e\phi(z)}{k_B T}$$

So, coming back to modified Nernst-Planck equation:

$$D_i\nabla c_i + z_i\mu_{m,i}Fc_i\left(1-\frac{\sum_j^M 10^3 z_j v_j N_A c_j^b \exp\frac{-z_j e\phi(z)}{k_B T}}{z_i(1+\sum_j^M 10^3 v_j N_A c_j^b(\exp\frac{-z_j e\phi(z)}{k_B T}-1))}\right)\nabla\phi = 0$$

Finally, substituting $\mu_{m,i}$ with $\mu_{m,i}^s$ defined as:

$$\mu_{m,i}^s = \mu_{m,i}\left(1-\frac{\sum_j^M 10^3 z_j v_j N_A c_j^b \exp\frac{-z_j e\phi(z)}{k_B T}}{z_i(1+\sum_j^M 10^3 v_j N_A c_j^b(\exp\frac{-z_j e\phi(z)}{k_B T}-1))}\right) \tag{1.8}$$

A new modified Nernst-Planck equation can be written as:

$$\frac{\partial c_i}{\partial t} + \nabla(c_i\boldsymbol{u}) - \nabla(D_i\nabla c_i + z_i\mu_{m,i}^s Fc_i\nabla V) = R_{chem,i} \tag{1.9}$$

1.3.3 Surface charge density

Different theories are proposed in literature to define the surface charge density assumed by a solid and reactive material in contact with an electrolyte solution. Both Pardon and Jiang have proposed a simply definition of its value expressed in eq. 1.10 [7, 17]. The described model, called Multisite Complexation (MUSIC), was developed by Hiemstra [18].

$$\sigma_s = -\frac{e\ Nt}{1 + \frac{c^s_{H^+}}{10^{-pKa}}} \tag{1.10}$$

σ_s is the surface charge density expressed with C/m^2 unit, Nt is the distribution of binding sites on the surface, $c^s_{H^+}(M)$ the molar concentration of H^+ ions (more precisely H_3O^+ as it will explained in the further section) next to the surface where chemical reactions take place and $pKa = -\log_{10} Ka$ with Ka as acid dissociation constant.
This equation assumes that the only reaction that takes place at solid-liquid interface is only the first of these two reactions:

$$\mathrm{AOH} \xleftrightarrow{\mathrm{Ka}} \mathrm{AO^-} + \mathrm{H_s}^+$$
$$\mathrm{AOH_2}^+ \xleftrightarrow{\mathrm{Kb}} \mathrm{AOH} + \mathrm{H_s}^+$$

Kb is the basic dissociation constant. The second reaction was not considered in the final study because the commonly used materials in these applications, as silicon dioxide, usually expose only negative charges [10]. But its functioning is compared with MUSIC model in the next chapter.
Nt value depends on the material in contact with solution. Different materials expose different numbers of binding sites, for example silicon dioxide can expose a site density $Nt \sim 1.5\ 1/nm^2$ [19]. But it is possible to find different ranges of values in literature.
Generally, it is experimentally measured that σ_s value is around $-(1-100)\ mC/m^2$ for latter dielectric [20]. Other materials, as silicon carbide, which will be tested in model validation with experimental data, experimentally show much lower values (around $-0.2\ \mu C/m^2$ [10]), which means a much lower Nt (e.g. $Nt = \frac{-0.2\ \mu C/m^2}{e} = 1.25 * 10^{-6}\ 1/nm^2$).
If also basic dissociation reactions are wanted to be simulated, a similarly simply equation to define the surface charge density value was developed by Yates [21] and presented by Taghipoor in his study [19] where also Kb constant was considered. His equation is reported here below.

$$\sigma_s = e\ Nt \frac{Kb\ c^s_{H^+} - \frac{Ka}{c^s_{H^+}}}{1 + Kb\ c^s_{H^+} + \frac{Ka}{c^s_{H^+}}} \tag{1.11}$$

Different values for pKa and pKb can be founded in literature, for example 6.3 and 0.3 respectively [19], or 7.5 for pKa in Jiang's study [17].
For all this thesis, each equation for surface charge density is used with its respective pKa and pKb, if present. So, eq. 1.10 will use $pKa = 7.5$ and eq. 1.11 with $pKa = 6.3$ and $pKb = 0.3$. In validation section, the chosen equation to reproduce experimental results and its motivations are described.

Chapter 2

FEM description

2.1 Model description

2.1.1 Model development

To reach the proposed goal, an initial literature research of current approaches was executed to define the general structure of the FEM. The purpose of this work was also to obtain an enough realistic and computationally easy-to-use model. For this reasons, some aspects, that physically happen and other models in literature simulate, have not been considered due to their negligible role.
Initially, focusing on Pardon's work, whose task was quite different from that one of this thesis, as aforementioned, a 2D model was developed taking account not only the two governing equations mentioned in previous chapter, Poisson and Nernst-Planck, but also Navier-Stokes equation to simulate fluid flow inside the nanochannel and its additional contribute to ions movement [7].
However, this initial model was rejected soon due to the unrealistic and unknown behavior. The problem was initially treated with a too much high level of complexity.

For this reason, to study in the most precise way every physic contribution, a simpler model was developed in a single dimensional space. This model simulated the ionic and electric potential distributions on the normal direction from the channel wall. Only electrostatic and ions movement physics were been studied due to the flux of fluid was impossible to simulate at this dimension and this direction. Furthermore, when fluid flux is considered as zero like in a stationary study, contribute of Navier-Stokes equation can be considered as negligible [22].
In this initial model it was impossible to consider the diffusion of ions from a high concentration reservoir to an empty sink as in the proposed task due to the not present direction of diffusive movement, axial to channel.
This model was initially developed as those one in literature, using the classical

Poisson-Nernst-Planck coupled equations aforementioned. However, the model was not able to simulate the realistic saturation of counter-ions once reached the maximum concentration. For this reason, the mobility term for each ionic species was modified with eq. 1.8 to obtain the modified Nernst-Planck equation above shown.
Then, the obtained model was implemented to bi-dimensional space. Due to this pursuit, also the diffusion of ions through the channel was allowed. The fluid flux was kept negligible due to the assumption that when only a diffusion phenomenon is present, because drain-source voltage is not applied, the flux of solution is almost zero [22, 13].

2.1.2 General description

The two final models aforementioned, the single dimension and the bi-dimensional ones, are here described and compared. An especial focus is kept on the latter due to its higher complexity.
All the models presented and tested were developed as stationary studies of task phenomenon. Indeed, a time-dependent study was not chosen as final version due to the impossibility of a fully coupling of modules that solve Nernst-Planck and Poisson equations respectively and they had to be solved differently decreasing the precision of the solution. Instead, in stationary study, a fully coupling of governing equations was always allowed. Furthermore, the modified Poisson-Nernst-Planck equation obtained using mobility term described in equation 1.8 is calculated for steady state conditions, so it could lead to a wrong behavior if used in a time-dependent study.

2.2 Geometry and materials

In this simulation three different types of materials have been considered:

fluid domain it is define in sink, in the reservoir (in 2D model) and in the channel domain, water is chosen as solution, its relative permittivity is set at 80;

dielectric domain it is the dielectric layer between the electrode, that externally applies the electric potential, and Stern layer. Silicon dioxide is usually used with a relative permittivity of 4.2, but also silicon carbide, with a relative permittivity equal to 9.7, is tested;

Stern layer it is differentiated from first material due to its different structure, composed by adsorbed ions with the solid surface. Its relative permittivity is different from fluid domain, it has a distributed capacity equal to 0.3 F/m^2 [23] and its relative permittivity is obtained as $\frac{0.3\ F/m^2\ *\ 0.3\ nm}{\epsilon_0} \approx 10$.

2.2.1 1D model

1D model simulates the normal direction from charged wall. The different materials which compose the line are here sequentially listed:

dielectric layer with *dielectric* thickness;

Stern layer with 0.3 nm thickness;

channel filled with solution, *dim* large;

Stern layer with 0.3 nm thickness;

dielectric layer with *dielectric* thickness;

dielectric and *dim* are parameters that are changed to evaluate the model and test it on experimental data.

2.2.2 2D model

2D geometry is shown in figure 2.1. Each component (reservoir, channel and sink) is built as here described:

Reservoir and sink squares with 10 μm sides;

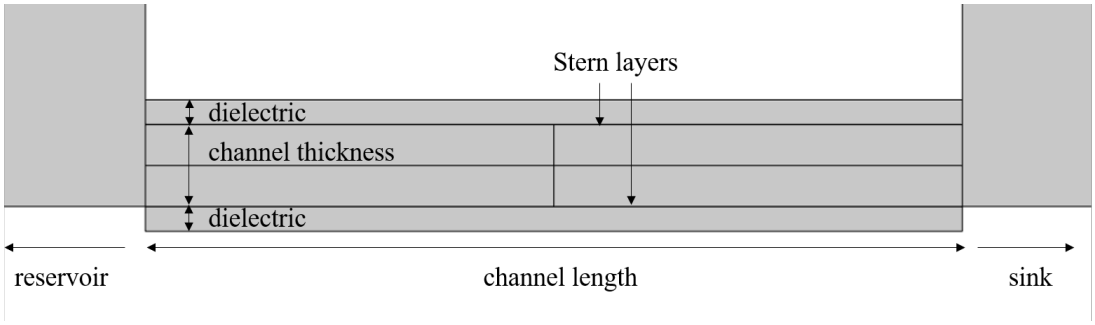

Figure 2.1: 2D geometry from COMSOL model

Channel rectangle 1 μm long and dim high, placed between the previous chambers;

Dielectric layers two rectangles 1 μm long and $dielectric$ high;

Stern layers two rectangles 1 μm long and 0.3 nm high, they are placed between each dielectric layer and channel side.

2.3 Physics

Two physics modules are used in this study, Electrostatics and Transport of Diluted Species, to solve equations 1.3 and 1.9, respectively.

Electrostatic module is defined in all geometry domains. In 1D model, this module is fully coupled with the other, in a steady state study. For this reason, the space charge density equal to $10^3 N_A \sum_i e c_i z_i$ is obtained as result from Transport of Diluted Species physics. In 2D model the same structure is maintained, adding some new boundary conditions due to the different and more complex geometry.

Five different ionic species are considered: H_3O^+, OH^-, Na^+, Cl^- and the charged drug. Obviously, positive or negative unitary charges are defined for each species but drug has a variable charge. H_3O^+ is used instead of H^+ because the latter species does not exist inside an electrolytic solution where it recombines immediately to form H_3O^+ [24]. Three Transport of Diluted Species physics are used, two for the couples H_3O^+/OH^- and Na^+/Cl^-, respectively, the last one is used for drug species. All these physics are defined for the fluid domain, but H_3O^+/OH^- is the only couple that is defined also inside Stern layer domain, because it is commonly considered the only one couple of species that could enter inside this space due to their lower dimensions [7].
Default mobility defined by COMSOL is substituted with the new one used in eq. 1.8, $\mu^s_{m,i}$. In this way the Nernst-Planck equation defined in this physics obtains as results of distribution of concentrations at steady state conditions the concentration defined in eq. 1.7. In 2D model bi-dimensional matrix $\mu_{m,i}$ is used and shown here below.

$$\mu_{m,i} = \begin{bmatrix} D_i/RT & 0 \\ 0 & \mu^s_{m,i} \end{bmatrix} \tag{2.1}$$

So, the new bi-dimensional Nernst-Planck equation will solve along x direction, axial with the channel, a normal diffusive study, and along y, normal to channel walls, a study equivalent to that one obtained with 1D study.
ϕ term in NP equations solved by these physics is obtained as results from Electrostatic module. H_3O^+/OH^- couple is considered as point-like and, for this reason, their mobility is maintained as default.
Fixed ionic diameter are chosen for Na^+ and Cl^- equal to 0.184 nm and 0.121 nm, respectively [25].

The D_i value used by COMSOL has been left as default. Indeed, in a steady state study this variable has no relevance as shown in Nernst-Planck equation at steady state conditions.

2.4 Boundary conditions

2.4.1 1D model

In table 2.1 the boundary conditions that are imposed in 1D model are listed.
Two space density (ρ_{el}) nodes are defined in Electrostatic module, one for the fluid domain, where H_3O^+, OH^-, Na^+, Cl^- and drug are present, and another one for Stern layers where there are only H_3O^+ and OH^- ions.
ϕ_0 is the variable defined for the externally applied electric potential at the gate electrode.
Each ionic species bulk concentration, c_i^b, which is imposed as boundary conditions for NP modules and used in eq. 1.6 and 1.7, are listed in table 2.2. To maintain the electroneutrality of the solution when no external electric potential is applied, salt species are used as buffer of the solution, compensating the other negative or positive charges [23].
A specific condition about drug charge sign is imposed, as it is shown in aforementioned table, to always obtain positive concentrations even at high drug valences. Indeed, Na^+ or Cl^- compensates the external molecules if the latter assumes, when it is diluted in a solution, a negative charge or a positive one, respectively.
C_{salt} and C_{drug} are variables used to define salt species and drug bulk concentrations, respectively. The first one is defined as $C_{salt} = c\ 137\ (mM)$ where c is

Equation	**Location**	**Expression**
Poisson	Fluid domain	$\rho_{el} = 10^3 N_A \sum_i e c_i z_i$
	Stern layers	$\rho_{el} = 10^3 N_A \sum_i e c_i z_i$
	Dielectric external sides	$\phi = \phi_0$
	Dielectric-Stern interfaces	$\sigma_s = eq\ 1.10\ or\ 1.11$
NP H_3O^+/OH^-	Channel center (z=h)	$c_{H_3O^+} = eq.1.6(h)$
		$c_{OH^-} = eq.1.6(h)$
	Dielectric-Stern interfaces	$\boldsymbol{J}_{\perp,i} = 0$ (No Flux)
NP Na^+/Cl^-	Channel center (z=h)	$c_{Na^+} = eq1.7(h)$
		$c_{Cl^-} = eq\ 1.7(h)$
	Stern-Fluid interfaces	$\boldsymbol{J}_{\perp,i} = 0$ (No Flux)
NP drug	Channel center (z=h)	$c_{drug} = eq\ 1.7(h)$
	Stern-Fluid interfaces	$\boldsymbol{J}_{\perp,i} = 0$ (No Flux)

Table 2.1: Boundary conditions in 1D model

Conditions	Species	Expression (M)
$pH < 7$ *and* $z_{drug} > 0$	H_3O^+	10^{-pH}
	OH^-	$10^{-(14-pH)}$
	Na^+	C_{salt}
	Cl^-	$C_{salt} + 10^{-pH} - 10^{-(14-pH)} + z_{drug}C_{drug}$
	Drug	C_{drug}
$pH < 7$ *and* $z_{drug} < 0$	H_3O^+	10^{-pH}
	OH^-	$10^{-(14-pH)}$
	Na^+	$C_{salt} - z_{drug}C_{drug}$
	Cl^-	$C_{salt} + 10^{-pH} - 10^{-(14-pH)}$
	Drug	C_{drug}
$pH \geq 7$ *and* $z_{drug} > 0$	H_3O^+	10^{-pH}
	OH^-	$10^{-(14-pH)}$
	Na^+	$C_{salt} - 10^{-pH} + 10^{-(14-pH)}$
	Cl^-	$C_{salt} + z_{drug}C_{drug}$
	Drug	C_{drug}
$pH \geq 7$ *and* $z_{drug} < 0$	H_3O^+	10^{-pH}
	OH^-	$10^{-(14-pH)}$
	Na^+	$C_{salt} - 10^{-pH} + 10^{-(14-pH)} - z_{drug}C_{drug}$
	Cl^-	C_{salt}
	Drug	C_{drug}

Table 2.2: Bulk concentration values for 1D study

a coefficient used to modify salt concentration inside the solution. 137 (mM) is chosen as NaCl molar concentration value in PBS solution, commonly used during experimental test to reproduce physiological environment. Only NaCl is considered as basic component of PBS to simplify the software functioning. During this thesis it will be usually used terms as 0.01xPBS (also 1%PBS) or 1xPBS. They mean that salt concentration inside the solution has a c value equal to 0.01 or 1, respectively.

2.4.2 2D model

Boundary conditions for 2D model are listed in table 2.3. In two dimensional study, new fixed concentrations are placed at external boundaries of sink and reservoir, these new conditions are named $c_{i,0}$. To correctly solve the modified PNP, a special

Equation	**Location**	**Expression**
Poisson	Fluid domain	$\rho_{el} = 10^3 N_A \sum_i e c_i z_i$
	Stern layers	$\rho_{el} = 10^3 N_A \sum_i e c_i z_i$
	Dielectric external sides	$\phi = \phi_0$
	Sink and Reservoir external sides	$\phi = 0$
	Dielectric-Stern interfaces	$\sigma_s = eq$ 1.10 or 1.11
	Remaining boundaries	$\nabla\phi_\perp = 0$ (Zero charge)
NP H_3O^+/OH^-	Sink and Reservoir external sides	$c_{H_3O^+,0} = c^b_{H_3O^+}$
		$c_{OH^-,0} = c^b_{OH^-}$
	Remaining external boundaries	$\boldsymbol{J}_{\perp,\boldsymbol{i}} = 0$ (No Flux)
NP Na^+/Cl^-	External Reservoir side	$c_{Na^+,0} = c^b_{Na^+,r}$
		$c_{Cl^-,0} = c^b_{Cl^-,r}$
	External Sink side	$c_{Na^+,0} = c^b_{Na^+,s}$
		$c_{Cl^-,0} = c^b_{Cl^-,s}$
	Remaining external boundaries	$\boldsymbol{J}_{\perp,\boldsymbol{i}} = 0$ (No Flux)
NP drug	External Reservoir side	$c_{drug,0} = c^b_{drug}$
	External Sink side	$c_{drug,0} = 0$
	Stern-fluid interface	$c_{drug} \leq c_{max}$
	Remaining external boundaries	$\boldsymbol{J}_{\perp,\boldsymbol{i}} = 0$ (No Flux)

Table 2.3: Boundary conditions in 2D model

boundary condition is placed on the external boundaries nearest to channel walls, the fluid-Stern layers interfaces, that imposes the concentration of studied drug at most equal to its maximum concentration c_{max} or less. This condition is imposed only for drug species because is the only one that could reach the saturation limit, differently from salt ions.
Due to the presence or not of charged drug in each domains, buffer compensation of salt is different from that one explained in table 2.2. The new salt concentration bulk values are listed in table 2.4.

Conditions	**Name**	**Expression (M)**
$pH < 7$ *and* $z_{drug} > 0$	$c^b_{\mathrm{Na}^+,r}$	C_{salt}
	$c^b_{\mathrm{Na}^+,s}$	C_{salt}
	$c^b_{\mathrm{Cl}^-,r}$	$C_{salt} + 10^{-pH} - 10^{-(14-pH)} + z_{drug}C_{drug}$
	$c^b_{\mathrm{Cl}^-,s}$	$C_{salt} + 10^{-pH} - 10^{-(14-pH)}$
$pH < 7$ *and* $z_{drug} < 0$	$c^b_{\mathrm{Na}^+,r}$	$C_{salt} - z_{drug}C_{drug}$
	$c^b_{\mathrm{Na}^+,s}$	C_{salt}
	$c^b_{\mathrm{Cl}^-,r}$	$C_{salt} + 10^{-pH} - 10^{-(14-pH)}$
	$c^b_{\mathrm{Cl}^-,s}$	$C_{salt} + 10^{-pH} - 10^{-(14-pH)}$
$pH \geq 7$ *and* $z_{drug} > 0$	$c^b_{\mathrm{Na}^+,r}$	$C_{salt} - 10^{-pH} + 10^{-(14-pH)}$
	$c^b_{\mathrm{Na}^+,s}$	$C_{salt} - 10^{-pH} + 10^{-(14-pH)}$
	$c^b_{\mathrm{Cl}^-,r}$	$C_{salt} + z_{drug}C_{drug}$
	$c^b_{\mathrm{Cl}^-,s}$	C_{salt}
$pH \geq 7$ *and* $z_{drug} < 0$	$c^b_{\mathrm{Na}^+,r}$	$C_{salt} - 10^{-pH} + 10^{-(14-pH)} - z_{drug}C_{drug}$
	$c^b_{\mathrm{Na}^+,s}$	$C_{salt} - 10^{-pH} + 10^{-(14-pH)}$
	$c^b_{\mathrm{Cl}^-,r}$	C_{salt}
	$c^b_{\mathrm{Cl}^-,s}$	C_{salt}

Table 2.4: Bulk concentration values for 2D study

Part II

Results and discussion

Chapter 3

Model validation

3.1 Surface charge density

The surface charge density modelling is tested and compared with reference results without considering the presence of charged drug, because literature tests do not take into account its presence, but focus on the relationship between σ_s and variable environmental conditions (salt concentration and pH value).

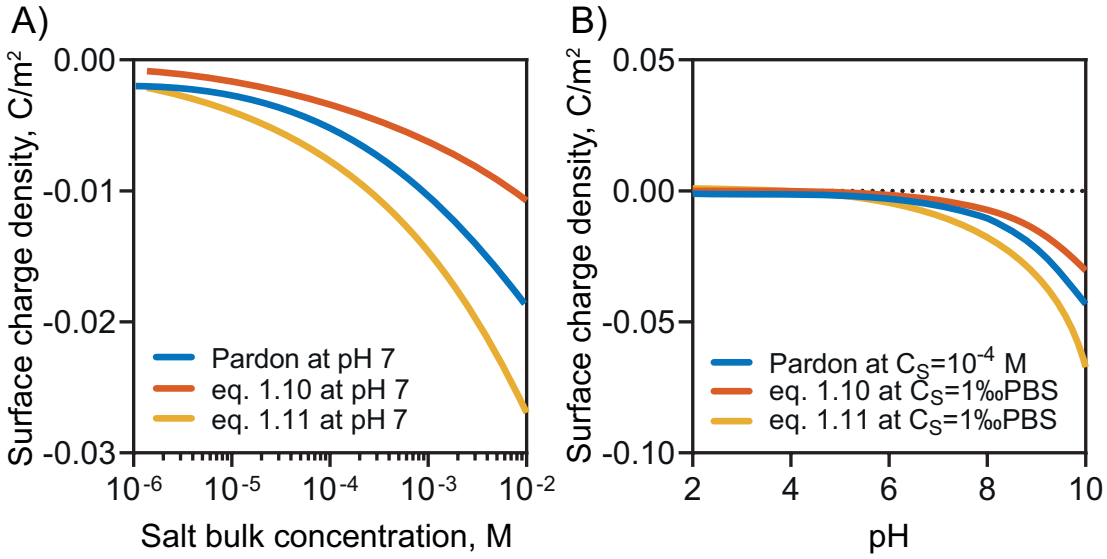

Figure 3.1: Surface charge density in relationship with bulk salt concentration (**A**) and pH (**B**). Reference results are obtained from Pardon [7]. No charged drug is present. Simulations performed in 1D model.

Initial tests shown in figures 3.1, 3.2 and 3.3 had been taken with a slightly different single dimensional FEM. In the model used for these validations, the salt and H^+/OH^- species were simulated in all fluid domain, also inside Stern layers, differently from Pardon's assumption [7]. This model was the first developed and tested to analyze surface charge simulation. The differences between this initial model and its behavior, and the final bi-dimensional model will be shown in figure 3.4.

To test only surface charge density and fit as much as possible reference results, ϕ_0 applied at external dielectric surface is set as zero.

In figure 3.1 it is possible to see the behavior of FE model when different conditions are imposed. In figure 3.1.A the results of model using equation 1.10 from Jiang [17] and eq. 1.11 from Taghipoor [19] are shown. In this figure the pH is set as 7 and different salt concentrations are tested. In figure 3.1.B the same equations are tested and compared with reference results ranging pH values in a 1‰PBS solution.
Both σ_s equations have a similar slope comparing with reference results.
To obtain these graphics, both equations 1.10 and 1.11 used the aforementioned value of 1.5 $1/nm^2$ as value for Nt parameter, assuming that the dielectric material used is silicon dioxide.

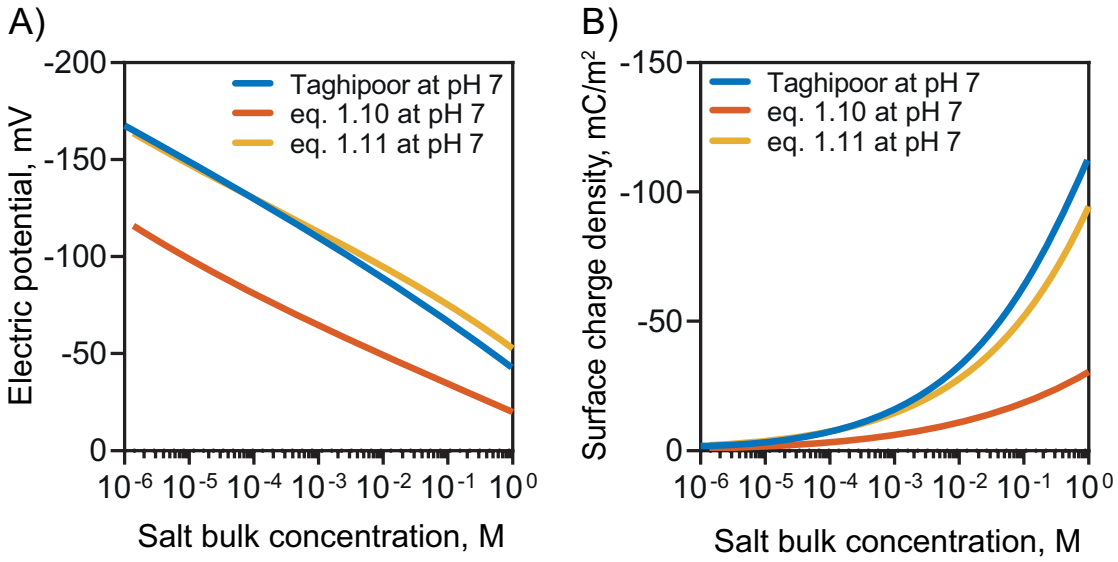

Figure 3.2: Stern layer potential (**A**) and surface charge density (**B**) in relationship with salt bulk concentration at pH equal to 7. Reference results are obtained from Taghipoor [19]. No charged drug is present. Simulations performed in 1D model.

In figures 3.2.A and 3.2.B the electric potential at Stern layer and surface charge density obtained changing salt concentration at pH equal to 7 are respectively shown. Model results obtained using eq. 1.11 fit very well with those from reference, more than those where eq. 1.10 is used. This better agreement is easily explained because eq. 1.11 is obtained from Taghipoor's work as the reference curves. However, Jiangs's equation shows a good fit with literature results as well. These simulations are performed with the same 1D model previously mentioned.

The last comparison is obtained measuring the electric potential and local pH value at solid-liquid interface in a 1‰PBS solution. The results are shown in figure 3.3.A and 3.3.B for electric potential and local surface pH, respectively. Here, Jiang's equation and Taghipoor's one, are compared with Pardon's results. As previous comparisons, the same single dimensional model is used without simulated charged drug.

Both equations show a good fit with reference results, but Taghipoor's equation causes the surface to assume also a positive charge density at extremely low pH values.
This behavior is rejected to simulate the main used dielectric material SiO_2 because it was experimentally measured that it assumes always a negative charge.

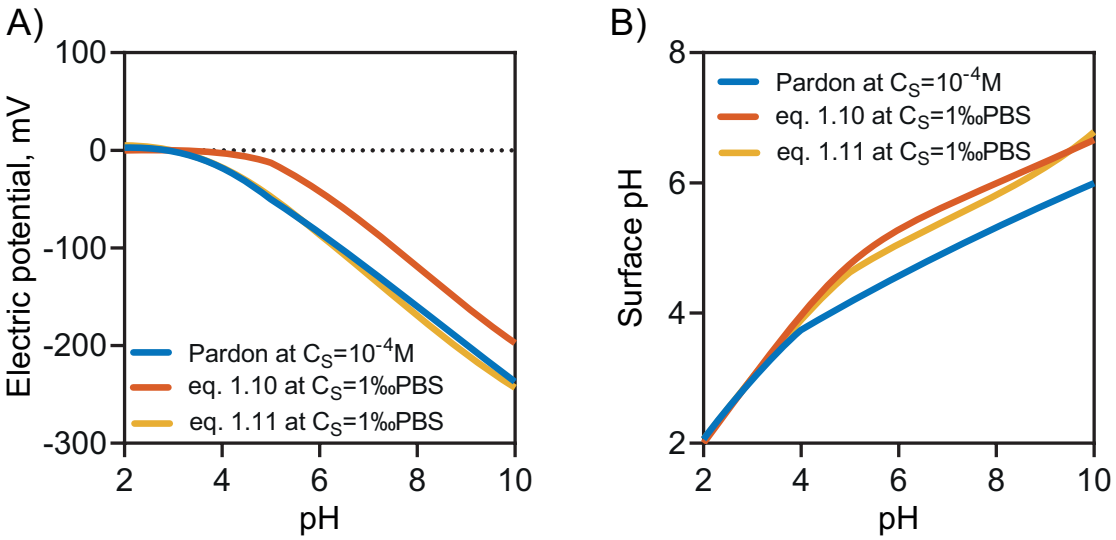

Figure 3.3: Surface electric potential (**A**) and surface pH (**B**) in relationship with bulk pH in a 10^{-4} M solution. Reference results are obtained from Pardon [7]. Simulations performed in 1D model.

Due this reason Jiang's equation is chosen to be used definitively to model σ_s in 1D and 2D models that simulate the exclusion or enrichment of charged drug.

Repeating the simulations of figure 3.1 with the final bi-dimensional model, figure 3.4.A shows the influence of assumption that no ions out of H_3O^+/OH^- species can enter inside Stern layer. Indeed, comparing the new results with those previously obtained, the maximum negative value assumed by the surface charge is decreased. This behavior can be caused by the fact that if in the initial 1D model the salt counter-ions could move next to the dielectric wall to screen its surface potential, in the new model only H_3O^+/OH^- species are allowed to move within the Stern layer, leading to a much higher number of these ions next to the solid-liquid interface than previous condition. Due to the chosen equation 1.10 used to calculate the surface charge density magnitude, its absolute value is inversely proportional to H_3O^+ concentration, so the maximum negative value is lower in final 2D model. This effect is more relevant when the presence of salt ions inside the Stern layer differs more from initial and final models, which means, at highest salt concentrations.

As it is shown in figure 3.4.B, introducing inside the simulation the presence of the drug, it leads to a higher absolute value of surface charge at lowest salt

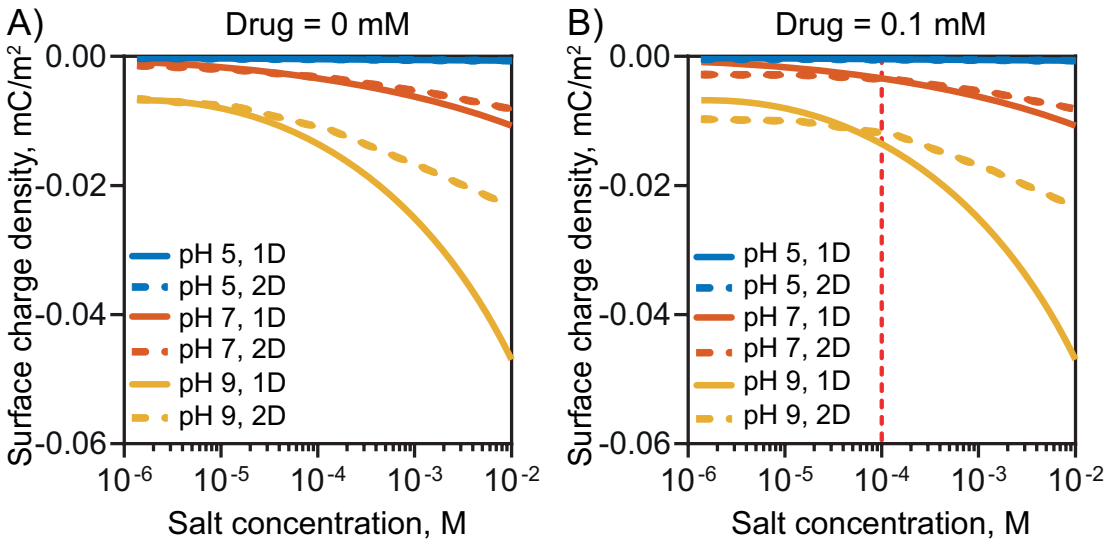

Figure 3.4: Bi-dimensional model validation of surface charge density without (**A**) or with (**B**) the presence of drug inside the solution at different salt concentrations and pH values. The results are compared with the results of the initial 1D model shown in figure 3.1.A

concentrations and an almost negligible change at highest ones. This behavior can be motivated by the compensation explained in table 2.4. Using a negative charged drug, at pH values higher than 7 or equal, the concentration of Na^+ is increased to compensate it. Consequently, a lower amount of H^+ is needed at the surface, which means a higher absolute value of surface charge density. The compensation effect is influential at salt concentrations lower than drug one, in this case $10^{-4}M$, when influence of effective PBS percentage term c is negligible. Indeed, at lowest salt concentration the real ionic strength of solution is less dependant from PBS percentages and a higher amount of ions screening the surface charge is present in the solution. Red vertical dashed line in figure shows the drug concentration value. Therefore, it is possible to see that at higher salt concentration values the influence of drug decrease more and more. On the other hand, at lower values, surface charge density is almost constant, due to the main influence of constant presence of drug which causes a constant salt species concentration, independent from PBS percentage.

3.2 Modified PNP

The most innovative aspect of this model is the implementation introduced by the modified Poisson-Nernst-Planck equations (mPNP). Using the term shown in equation 1.8, the model should rightly simulate the saturation of a not point-like counter-ion species next to the wall.
In figure 1.4.B the wanted behavior has been shown, obtained as the calculation of equation 1.7 directly from exponential voltage curve shown in figure 1.4.A. Here the results of fully coupled model with modified terms are tested and compared with previous figures.

The FE model used for the validation is the last developed bi-dimensional model previously described.

In this thesis it is not considered the case that the molecule size is larger enough to avoid its entrance into the channel, so its diameter is bigger than channel height. This assumption is leaded by the fact that modified ion mobility used in this FE model does not simulate this case. Indeed, equation 1.7 is built to correctly calculate concentrations of counter-ions saturation next to channel walls, because its denominator term becomes more important at highest potentials leading to a

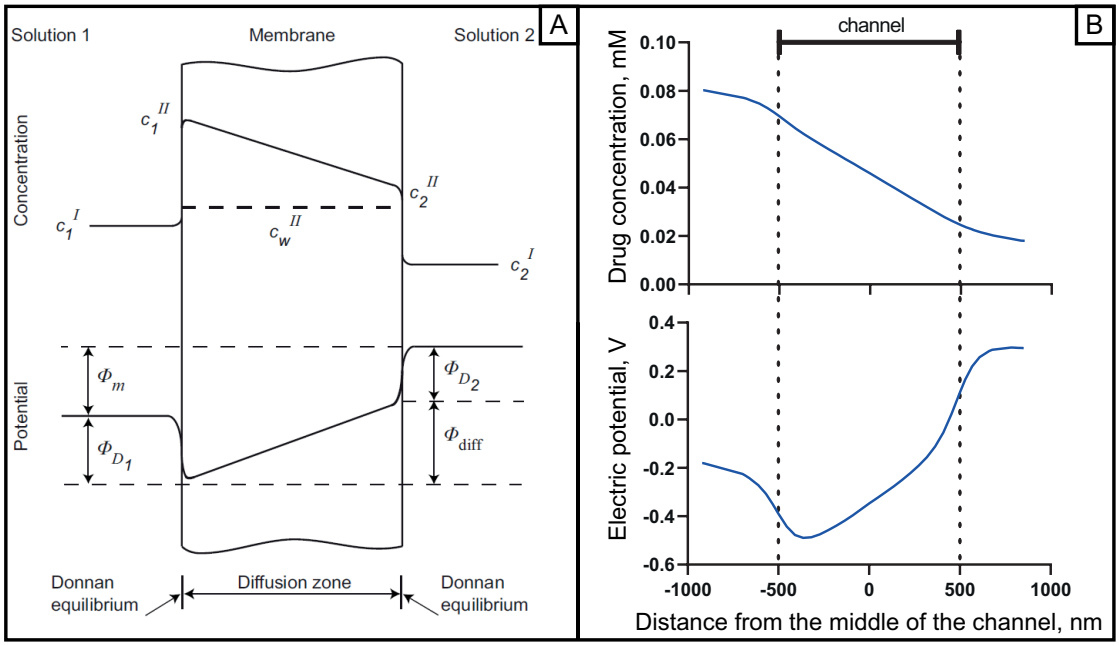

Figure 3.5: Donnan equilibrium shown by Schoch (**A**) and results obtained by the FE model (**B**) [9]. The simulated diffusing molecule is a co-ion.

saturation at maximum concentration value. If electric potential is zero, modified PNP does not affect concentration in considered location. So it cannot affect bulk concentration if EDL does not overlap in the middle of channel.
For this reason, in this validation it is not considered the co-ions concentration curve. It does not mean that the modified equation does not affect these ions in any case. Their concentrations are obviously unaffected if electric potential in calculated point is zero, but in the case of a diffusion between two chambers connected by a gated channel, electric potential inside, on axial direction, is not zero [9], as shown in figure 3.5.A. This phenomenon is known as Donnan equilibrium between the electrophoretic force and diffusive one that takes place when two electrolytic solutions with a concentration gradient, are connected by a semi-permeable membrane. Indeed, if a specific charge is not allowed to pass inside the nanochannel, against diffusive force, the potential inside the nanochannel differs from zero and changes along channel axis.
In figure 3.5.B it is also possible to see the rightly reproduction of Donnan equilibrium obtained by developed FEM. Due to this not zero potential in the middle of nanochannel, equation 1.7 can affect ions distribution at the middle of nanochannel taking into account ionic sizes, if electric potential assumes an enough high value to allow denominator term to have a relevant role.
This effect is impossible to reproduce in a single dimension model due to the lack of diffusive force modelling.

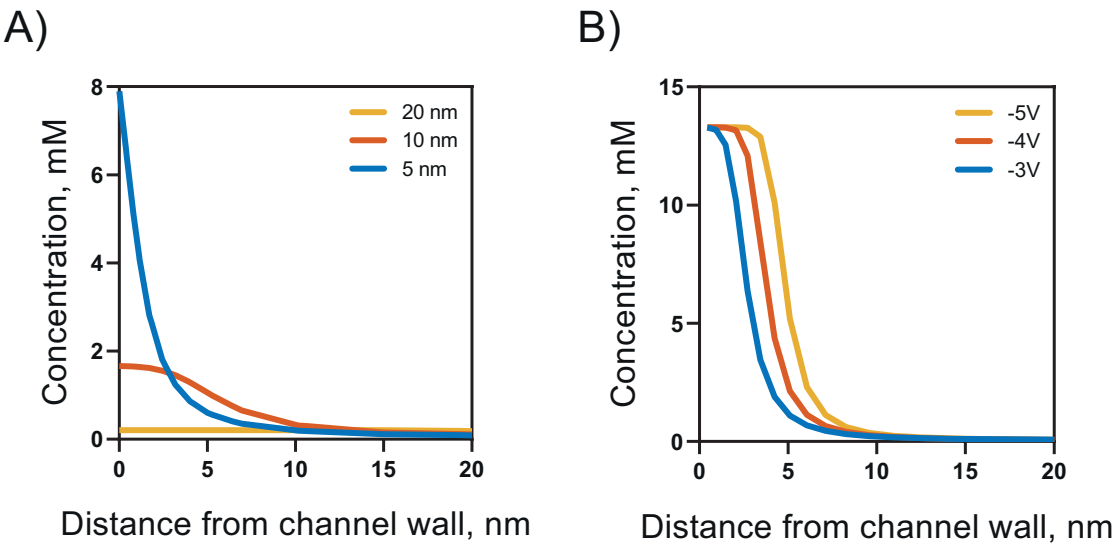

Figure 3.6: Concentration curves of drug molecules with different ionic diameters (**A**) and increasing the externally applied gate voltage with a constant drug diameter (**B**).

In figure 3.6.A it is possible to see the saturation of a counter-ion drug when the maximum concentration is relevant or not. Indeed, for a molecule whose diameter is 5 nm, its maximum concentration is 13.28 mM. In this case, with a sufficiently low drug valence, the molecule does not reach this value at the wall. On the other hand, increasing ionic diameter to 10 nm and 20 nm, maximum values become 1.66 mM and 0.21 mM, respectively. As it is shown in the same figure, once the maximum value is achieved, the concentration remains constant until the wall. In figure 3.6.B an interesting effect similar to Balzant's work takes place: the increase of EDL in case of not negligible finite-size counter-ions. Indeed, due to the saturation of molecules concentration, the increasing electric potential at the liquid solid interface would need a longer EDL to be screened [26].

Chapter 4

Model results

To evaluate the influence of the highest number as possible of parameters and to obtain more precise results, it will be used for all the simulation shown below, the last developed bi-dimensional model. Indeed, single dimensional model was chosen to not be used due to the lack of extremely important phenomenon as diffusion itself of charged drug.

4.1 Membrane properties effects on V_{surf}

In this section the effect on dielectric surface potential of an externally applied one or leaded by the natural surface charge of material in contact with electrolyte solution is analyzed and discussed.
The aforementioned two cases that usually induce the EDL formation in the channel are separately focused and their both effects on the effective potential at solid-liquid interface (Surface Potential - V_{surf}) are analyzed. When a voltage is externally applied, the main aspects that affect its effect on surface potential are the dielectric layer thickness placed between the electrode and the solution and its permittivity, depending on used material. Other parameters as ionic strength of solution, as it will be demonstrated, have not such an influence in this case. On the other hand, if the electric potential is caused by the surface charge induced by chemical reactions between dielectric material and fluid, the number of reactive sites on the interface, ionic strength and pH of solution are the most important parameters that mainly affect its value and therefore the surface potential. The interaction of these two contributions is also studied due to the not trivial effect on surface potential when both are considered as not zero.

4.1.1 Binding sites density effects on V_{surf}

In figure 4.1.A the relationship between reactive site density Nt ($1/nm^2$) and respective V_{surf} expressed at solid-liquid interface is shown. Different salt concentrations are tested, ranging from 0.1‰PBS to 10xPBS. The concentration of charged drug is maintained at zero and the pH value of the solution is 7. As already confirmed by figure 3.2.A, dielectric surface becomes more negative as much the salt concentration is lower. The curves highly decrease at first density values and then they become slightly linear. In figure 4.1.B the previous relation is analysed changing solution pH from 5 to 9 and maintaining the salt concentration at 1%PBS. Drug concentration is again set as zero. As previously shown in figure 3.3.A, a higher value of pH leads to a higher surface potential absolute value. In both graphs of figure 4.1, V_{surf} hugely drops down at first density values until reaching a value where a linear relation with Nt starts. Because used eq. 1.10 has been developed to reproduce silicon dioxide charging, surface potential caused by chemical reactions is always considered as negative. A different type of dielectric material will need a different equation to adjust these phenomena.

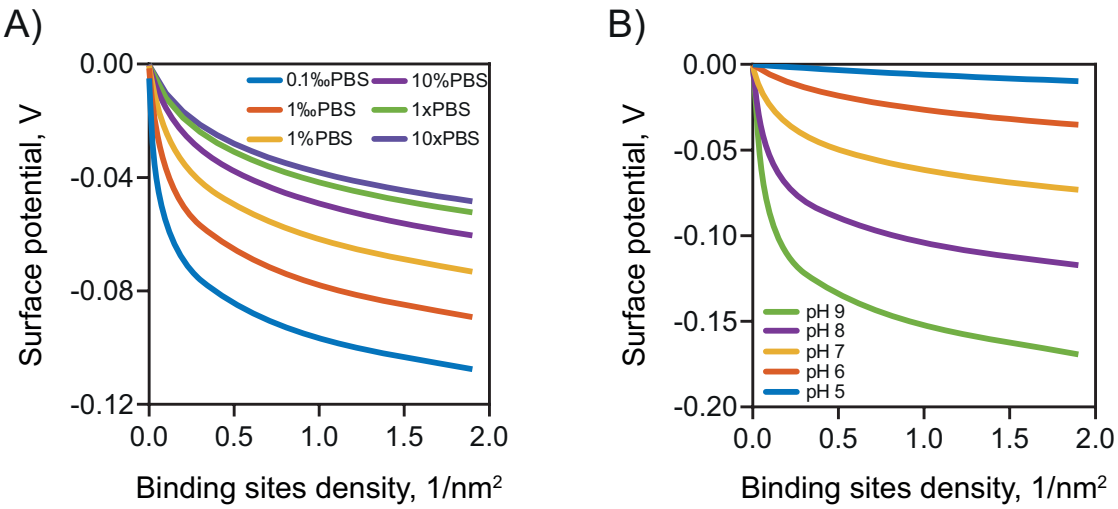

Figure 4.1: Simulations performed in a 150 nm large channel without an externally applied potential to test reactive sites density effect on V_{surf}. Drug concentration is zero. **A**: different salt concentrations are tested at pH value of 7. **B**: different pH values are tested in a 1%PBS solution.

4.1.2 Dielectric material properties effects on V_{surf}

In figure 4.2 the influence of dielectric material properties is tested at different conditions, especially the relevance of dielectric thickness and its electrical permittivity are focused. The drug concentration is still set as zero, the pH value as 7. To separately consider these effects from surface charge density, in all graphs of figure 4.2, reactive site density is zero, which means that surface density is zero as well.

In figure 4.2.A, the gate voltage at the electrode is ranged from 2 V to 10 V and its contribution to surface potential is shown at different dielectric thicknesses, that is tested from the lowest values of 1 nm to the highest ones of 30 nm. Dielectric material in this graph is silicone dioxide.
Relation between gate voltage and V_{surf} is quite linear, whose angular coefficient is dependent from dielectric thickness. Indeed, thin dielectric layer leads to a higher coefficient, which means that it is possible to obtain a higher modulation on surface potential through an externally applied potential.
4.2.B shows how dielectric thickness, here considered as SiO_2, influences V_{surf} maintaining gate voltage equal to 6 V and changing salt concentration. As it is possible to see, salt concentration is not extremely relevant when only an external

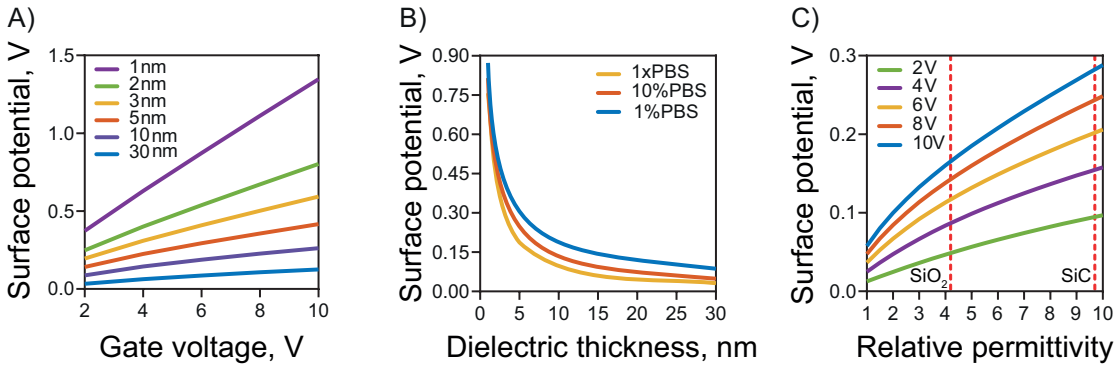

Figure 4.2: Simulations performed in a 150 nm large channel to show the effects of an electric potential applied to the gate electrode on surface potential at different dielectric material conditions. All the simulations maintain pH value as 7. The dielectric material is considered as not reactive with the solution (Nt=0). Drug concentration is zero. **A**: in a 1%PBS solution, V_{surf} trend depending on externally applied voltage at different SiO_2 layer thicknesses. **B**: relevance of silicon dioxide thickness on V_{surf} at different salt concentrations maintaining gate voltage at 6 V. **C**: influence of relative permittivity of used dielectric material on V_{surf} at different applied gate voltages. This simulation is performed in a 1%PBS solution and dielectric thickness is 20 nm.

voltage is applied. Decreasing the thickness of dielectric layer the electric potential that is transmitted at solid liquid interface is increased exponentially.
In figure 4.2.C it is considered the case that not silicon dioxide is used as dielectric material. Indeed, performing the simulations at salt concentration equal to 1%PBS, the effect on surface potential of different relative electrical permittivities is tested at different gate voltages. In these tests, the dielectric thickness is maintained as constant equal to 20 nm, ranging its permittivity from 1 to 10. The ϵ_r used to simulate silicon dioxide is 4.2 as highlighted by left vertical red dashed line; on the other hand, also silicon carbide, the dielectric material used in manufacturing process of experimentally tested nanofluidic membrane, is pointed out with the right red line to evidence the results obtained with ϵ_r equal to 9.7. As it is possible to see from figure 4.2.C, the relationship between ϵ_r and V_{surf} is slightly linear, whose angular coefficient depends in direct proportion on applied voltage at electrode.

4.1.3 Interaction between V_{gate} and σ

Finally, in figure 4.3, the case where both gate voltage and surface charge density are present is considered. Indeed, unexpectedly, the contributions of both terms on

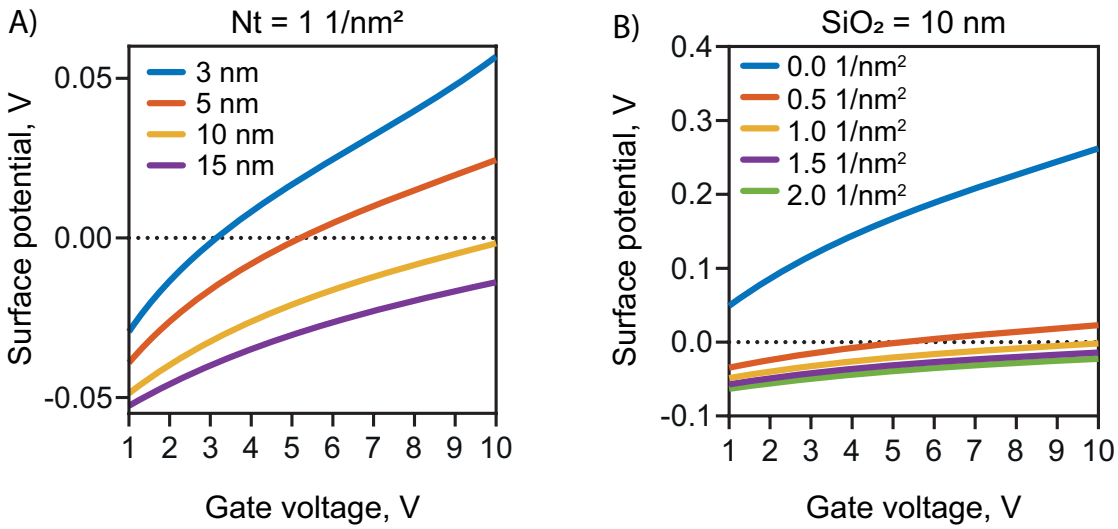

Figure 4.3: Effect of gate voltage on surface potential with different dielectric thicknesses and reactive binding sites densities with both non-zero values. The used solution is 1%PBS with pH equal to 7. Drug concentration is zero. **A**: with a fixed Nt value equal to 1 $1/nm^2$, different SiO_2 thicknesses are tested. **B**: with a fixed SiO_2 thickness value equal to 10 nm, different reactive binding sites density values are tested

surface potential can not be simply summed to obtain the real value. In this figure the simulations are performed using a solution with a salt concentration equal to 1%PBS and a pH of 7, the dielectric material used is silicon dioxide with a ϵ_r equal to 4.2. No drug is present in these simulations. In figure 4.3.A the surface potential values in relationship with gate voltage are shown maintaining Nt value equal to 1 $1/nm^2$ and different dielectric thicknesses are tested. *Vice versa*, in figure 4.3.B the ranged parameter is Nt and dielectric thickness is set at fixed value of 10 nm .

A simple example of the wrong assumption of the summation of effects is presented: if a gate voltage of 6 V is applied to a 10nm-thick silicon dioxide layer, in contact with a solution which has a salt concentration equal to 1%PBS, 7 as pH value and the oxide surface expose a binding sites density equal to 1 $1/nm^2$, from figures 4.1 and 4.2 the V_{surf} values of -0.06 V and 0.19 V are respectively obtained. However, the real value obtained by the direct simulation with the parameters listed above is -0.016 V and not 0.13 V as expected by the sum of previous two results.

Nevertheless, other observations could be obtained from this figure: the relation between V_g and V_{surf} is generally linear and maintaining as constant the dielectric thickness, the increase of Nt value leads to a decrease of the offset and also angular coefficient. On the other hand, at fixed Nt values, the variation of dielectric thickness influences only latter index, as shown in figure 4.2.A. This difference of effects is explained by the fact that at zero gate voltage, the only relevant parameter is Nt that can induce a not zero surface potential.
In any case, the relevance of surface charge not only on the offset of linear relationship between V_g and V_{surf} leads to the impossibility of summation of singular effects previously demonstrated.

To invert the polarity of a naturally negatively charged channel using an external potential, the right combination of sufficiently high gate voltage and enough low dielectric thickness with low reactive surface is needed.

4.2 Membrane properties effects on EEF

All simulations shown in this section are performed using a ±1 charged drug to simulate co- and counter-ions behaviors, respectively. The drug bulk concentration in the reservoir is imposed as 1 mM. The simulated drug has a ionic diameter of 1 nm. These parameters related to the drug are maintained as fixed in this section, and others about membrane properties, as channel dimension, are studied at different environmental conditions.
Because the applied potentials used for all simulations are directly imposed at the solid-liquid interface of the channel and the influence of surface charge density on V_{surf} itself has been previously studied, dielectric layer is set as not reactive, with a Nt value equal to 0. For this reason, also the pH of the solution is fixed at 7. Indeed, its relevance was previously demonstrated as relevant mainly for surface charge density, but if chemical reactions at the surface are not present, pH value can be considered as negligible.

4.2.1 Surface potential effects on EEF

In figure 4.4.A and 4.4.B different salt concentrations are tested, from 0.1‰PBS to 1xPBS, and the electric potential directly imposed at solid-liquid interface ranges from 0 to 1.2 V which is barely the same surface potential obtained with a 1nm-thick

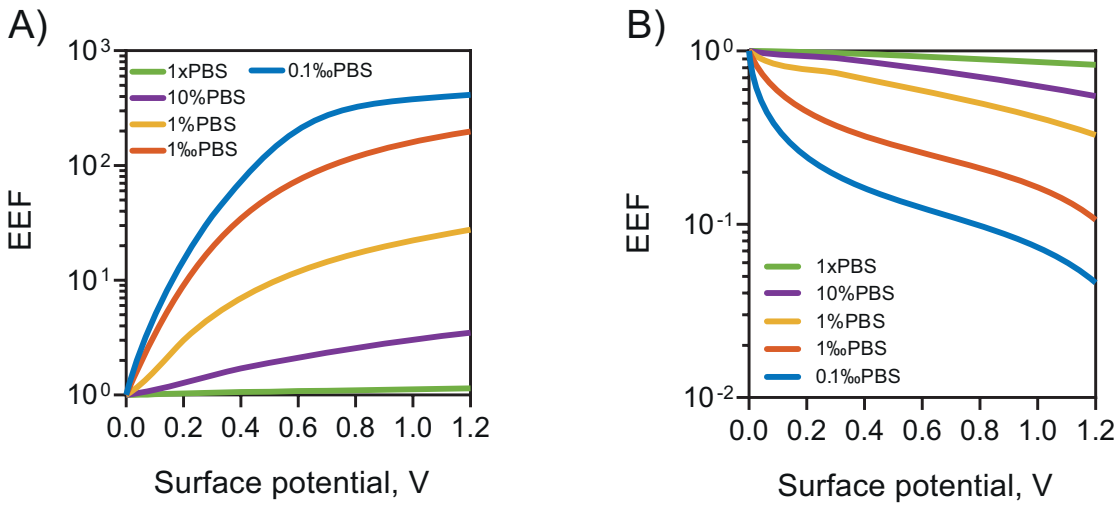

Figure 4.4: V_{surf} effects on EEF of charged drug. Channel width is 150 nm. Drug bulk concentration is 0.1 mM. pH of solution is 7. Counter-ions (**A**) and co-ions (**B**) EEF depending on V_{surf} at different salt concentrations.

silicon dioxide layer and a gate voltage of 10 V as shown in figure 4.2.A. Obviously in biomedical application a so high gate voltage could be unacceptable due to the power consumption and risks related to a so high applied voltage in an active implantable device, but to test the limit conditions these values are considered as well [27].
From the comparison of both images, the asymmetry of behaviors between co- and counter-ions is evident. Indeed, the maximum enrichment factor, obtained at the lowest salt concentration as expected due to the longest EDL, is about 40000%. On the other hand, the maximum exclusion factor is around 0% (which means a depletion of almost 100% of drug). This behavior is obviously caused by the inferior limit for co-ions at 0. For counter-ions, instead, the only limit is the maximum packaging concentration, which is difficulty achievable at drug diameter used in these simulations equal to 1 nm. Considering, as previously explained, molecule with a cubic shape, whose side is equal to ionic diameter, the maximum achievable concentration is 1661 mM, but, for a drug with a bulk concentration of 0.1 mM in the reservoir, the maximum concentration reached is 750 mM at the highest tested voltage of 1.2 V and in the 0.1‰PBS solution.

It is shown in aforementioned figures that co-ions curves at small surface potentials, especially at lowest salt concentrations, rapidly drop down, then their trend becomes slightly linear. The huge decrease at initial voltages could be caused by the immediate effect on EEF of the not absolutely negligible EDL length that at the lowest salt concentration (0.1‰PBS=13.7$\mu M \sim 10^{-5} M$) leads to a Debye's length around 100 nm as listed in table 1.1. Indeed, its impact in a channel with a diameter of 150 nm as in these simulations causes an EDL overlap and an almost complete exclusion from the channel of co-ions, already at fist voltage steps. But for higher ionic strengths of solution, this effectiveness at lowest potentials does not appear and the relationship between surface potential and EEF is almost linear for all tested V_{surf} values.
Meanwhile, for counter-ions this different behavior between ionic strengths is not present but a continuous increase, but not linear, takes place increasing surface voltage, at least at lowest salt concentrations. Trend of curves at highest ionic strengths could be considered linear.

Considering a biomedical application, within an active implantable device in contact with physiological environment at pH equal to 7.4 and in a 1xPBS solution, both co- and counter-ions show a linear behavior with applied voltages, which means that it should be possible a proportional modulation of EEF using different gate voltages. The choice of using co-ions or counter-ions drug species depends on what is their efficient administration dose and what is the better option between increasing or decreasing their releases. Counter-ions and co-ions drugs provide

an enrichment and an exclusion of ±15%, respectively, at these environmental conditions and at highest surface potentials.
In this case, with such a linear behavior of the system, and the need to obtain the highest difference between the passive phase (when no external voltages are applied and supposing a negligible surface charge of dielectric layer) and the active one (when a positive or negative voltage is applied at the electrode), the best choice is the application of the highest gate voltage as possible.
For this reason, in manufacturing process it is better to obtain a dielectric layer as thin as possible to more efficiently transfer the external voltage on the solid liquid interface.
Both choices imply not negligible drawbacks: a higher applied voltage increases the power consumption of the device and consequently a shorter battery life, which should be around six month and a few years for these applications, and a thinner dielectric layer or at most its absence could lead to a faster degradation of device due to chemical reactions with solution [10, 16, 28].
But if these phenomena were not limited by physiological environment, it could be useful to take advantages from the initial drop down aforementioned for co-ions at low voltages. Indeed, at lowest salt concentrations it could be possible a huge difference between passive and multiple active phases if the applied surface potentials are enough low, which means lower applied gate voltages and a thicker dielectric layer, preventing device from excessive power consumption and degradation risk.

4.2.2 Channel dimension effects on EEF

Differently from previous section, here the influence on EEF of different parameters involved with channel manufacturing properties are analyzed. Indeed, for both counter- and co-ions, the importance of channel dimension on the exclusion/enrichment factor is simulated changing different parameters. The channel dimensions are ranged from 30 nm to 300 nm.

In first figures pair, 4.5, the salt concentration in the solution is varied, in the second pair, 4.6, the ranged value is the surface applied potential, finally, in pair of figures 4.7, the Stern layer capacitance is changed from default value of 0.3 F/m^2.

Generally, the expected behavior is a slight dependence of EEF on channel dimension, until the EDL overlap occurs or its length becomes comparable with channel diameter and this parameter assumes a more relevant role [29].

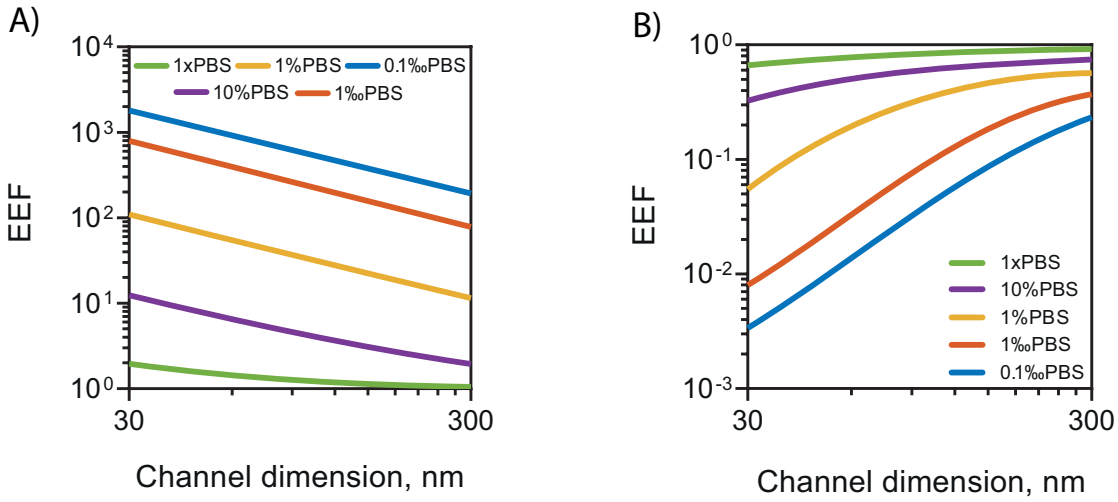

Figure 4.5: Channel dimension effects on EEF for both counter- and co-ions at different conditions. Counter-ions (**A**) and co-ions (**B**) EEF values are simulated for different salt concentrations, from 0.1‰PBS to 1xPBS. The surface potential is maintained constant at 1 V.

Solution ionic strength influence

As previously mentioned, in figures 4.5.A and 4.5.B the dimension of nanochannel is ranged at different PBS concentrations, that vary from 0.1‰PBS to 1xPBS, and its effect on EEF for counter-ions and co-ions is respectively shown. The surface potential used in these simulations is equal to 1 V. Obviously, decreasing the dimension of the channel, the influence of EDL on overall concentration of drug becomes more and more relevant. The trend is not linear but co-ions and counter-ions show different behaviors, the latter species shows that at different ionic strengths similar and proportional EEF values are obtained. Indeed, at logarithmic scale, curves at different PBS concentrations are almost parallel, decreasing if the percentage of PBS increases. The difference between each curve does not seem proportional to the change of ionic strength. The last curve in 1xPBS solution for counter-ions is not completely parallel to previous ones due to the inferior limit of 1.

Co-ions behave differently when the ionic strength of solution changes, probably due to the different effects of overlapping EDL that almost totally stop drug flux. Differently from counter-ions, the curves at different ionic strengths are not parallel, and their differences increase as smaller the channel is.
Indeed, as reported in table 1.1 by Schoch [9] and as already mentioned, at 0.1‰PBS and 1‰PBS Debye's length is around 100 nm and 30 nm, respectively. Indeed, the

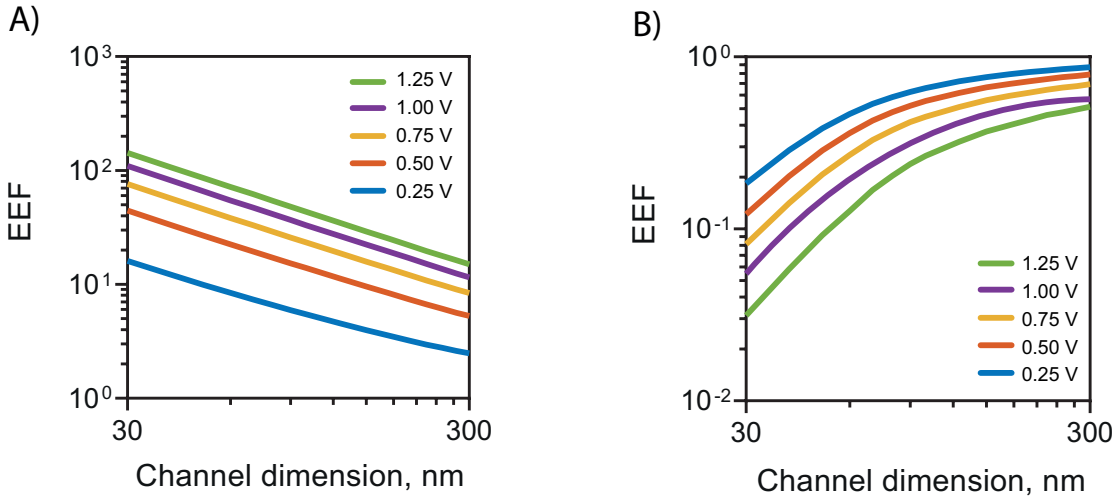

Figure 4.6: Channel dimension effects on EEF for both counter- and co-ions at different conditions. Counter-ions (**A**) and co-ions (**B**) EEF values are simulated for different surface potentials, which range from 0.25 V to 1.25 V. The tests are performed in a 1%PBS solution.

curves at these two PBS percentages present an almost stop of drug flux, considered at EEF value of 0.05, at 125 nm and 70 nm, respectively. The channel dimensions are not exactly the double of Debye's lengths aforementioned, but the simulations trend is indicative as well. At higher salt concentrations, as 1%PBS, where the λ_D is around 10 nm, only in 30 nm channels a similar depletion takes place due to the starting overlapping EDL. Higher percentages curves do not show this phenomenon yet.

V_{surf} influence

In figures 4.6.A and 4.6.B the simulations on counter- and co-ions are respectively shown changing the applied surface potential from 0.25 V to 1.25 V for each channel dimension ranged from 30 nm to 300 nm as before. The salt concentration is maintained at 1%PBS for all simulations.

As previously noticed, counter-ions show a sort of regularity, at logarithmic scale, varying applied potential. Indeed, a higher potential seems leading to similar curve obtained with a lower one, maintaining the same trend. It has to be also noticed that the displacements between each curve is poorly proportional to potential differences.
Obviously, decreasing channel diameter the EEF increases in a not linear way. In

comparison with figure 4.5.A, it is evident that ionic strength has a higher relevance in the drug enrichment than applied potential that assumes a secondary role.

Co-ions show a different behavior than figure 4.5.B actually. Indeed, the curves at each potential are parallel as the previous focused figure and displacements between them are almost proportional to the differences between applied potentials. As aforementioned for counter-ions, also for co-ions the percentage of PBS represents a more relevant parameter than applied potential. But the change of V_{surf} leads to more predictable results than changing PBS concentration due to its higher proportional behavior.

For both graphs it has to be noticed that, as expected with a salt concentration equal to 1%PBS that leads to a λ_D equal to 9.6 nm, the main change of slope in both ions types is around 70 nm, where EDL starts involving approximately 30% of channel diameter. This effect is more visible for co-ions than counter-ions due to the different effects of an almost overlapping EDL previously explained on these species.
As expected, at fixed Debye's length, the influence of EDL becomes relevant at specific channel dimension, but, for bigger diameters, all curves show a poor dependence on this parameter.

Stern layer capacitance influence

In the last pair of figures of this section, 4.7.A and 4.7.B, which shows the counter- and co-ions behaviors, respectively, using the same channel diameter range as in previous graphs, different Stern layer capacitance densities are tested. For all the simulations previously done, this value was set equal to 0.3 F/m^2 as reported in literature [23]. But, different dielectric materials, due to their changing structures once they are in contact with electrolytes solution, could present a different Stern layer capacitance. Indeed, as reported by the experimental tests on the studied nanofluidic membrane, a dielectric material as silicon carbide, due to its higher porosity than the main used silicon dioxide, shows a larger surface area in contact with solution which causes a higher capacitance [11]. The experimental value obtained by Dr. Grattoni and Di Trani was six times higher than SiO_2. So the influence of Stern layer capacitance is studied ranging its value from 0.1 F/m^2 to 2 F/m^2.
In both figures, the PBS concentration and surface potential are chosen as 1% and 0.25 V, respectively.

As it is shown, both counter- and co-ions go through an increase of effectiveness

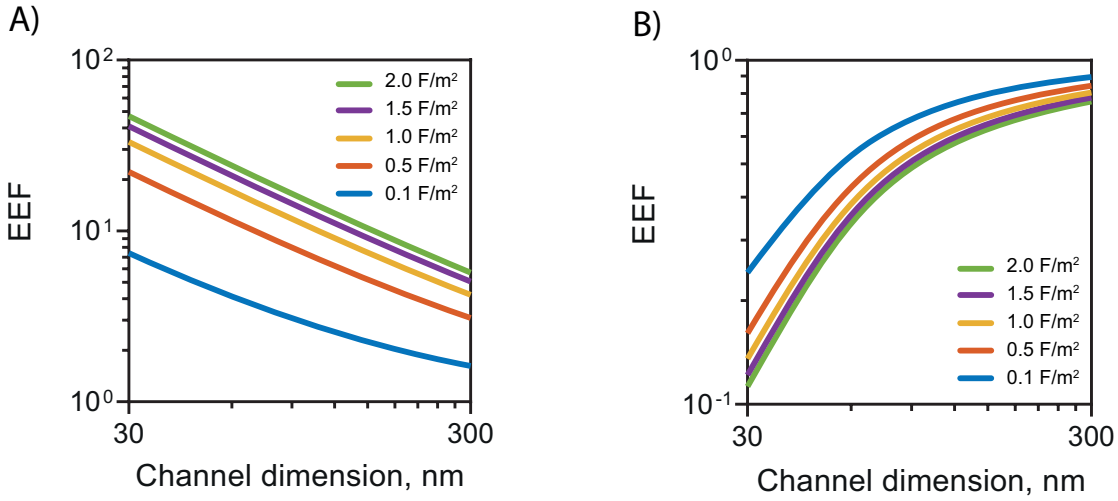

Figure 4.7: Channel dimension effects on EEF for both counter- and co-ions at different conditions. Counter-ions (**A**) and co-ions (**B**) EEF values simulated for different Stern layer capacity densities, that vary from 0.1 F/m^2 to 2 F/m^2. Surface potential and salt concentration are imposed as 0.25 V and 1%PBS, respectively.

of applied potential with a higher Stern capacitance. For both drug types, the difference between curves is not proportional with capacitance values shift. Anyway, the curves seem maintaining always the respective trends. In any case, this parameter is dependant on used material and it is not negligible on the overall influence on EEF.

4.3 Drug properties effects on EEF

The following section discusses the effects on enrichment/exclusion factor of those parameters dependent on drug properties such its valence, its bulk concentration in the reservoir and its ionic diameter. Indeed, thanks to the new ionic mobility term explained in the previous chapter, the proposed FE model can reproduce the saturation of counter-ions with a not negligible molecular diameter due to the achievement of maximum stacking concentration.

The consequences of considering the effective sizes of ions, especially when counter-ions assume a not negligible size and concentration saturation can be achieved, are interesting and cause variable effects on total enrichment of drug inside the channel at different environmental conditions.

In figures 4.8, 4.9, 4.10, 4.12 and 4.13 the tests are performed in 150 nm large channel, with a constant pH value of 7 and an externally applied voltage of $\pm 0.1\ V$ directly on solid-liquid interface. The channel surface is considered as not reactive, so Nt is zero. The other parameters as drug valence, its ionic dimension, its concentration in the reservoir and the salt one are varied to study their different influences on EEF of the drug.

4.3.1 Counter-ions saturation due to drug size

In figure 4.8 an unexpected but logically explainable phenomenon is shown. All graphs in figure are performed in a 1xPBS solution. For this reason the overall EEF range shown is low compared to enrichment factors seen in low PBS percentages curves in figure 4.5.A. The drug bulk concentration is equal to 0.1 mM for all simulations. In all graphs, drug diameters from 2 nm to 8 nm are tested.
In figure 4.8.A the counter-ion drug concentrations are shown along normal direction from channel wall when its valence is equal to 10 q. Different ionic diameters are tested and it is possible to see a decrease of maximum concentration reached by the drug as bigger its dimension is, as could be expected.
Nevertheless, in the second figure, 4.8.B, where the concentrations of other counter-ion not point-like species inside the solution, Na^+, are shown from the same simulation as previous figure, the concentrations next to the channel wall decrease with increasing drug dimension. The assumed explanation of this behavior is that monovalent salt ions result fewer concentrated next to channel wall because the even larger drug takes up space against other counter-ions species that are less attracted than latter highly charged molecules. Indeed, Na^+ ions decrease their concentrations next to the wall until zero at drug ionic diameter of 4 nm, value

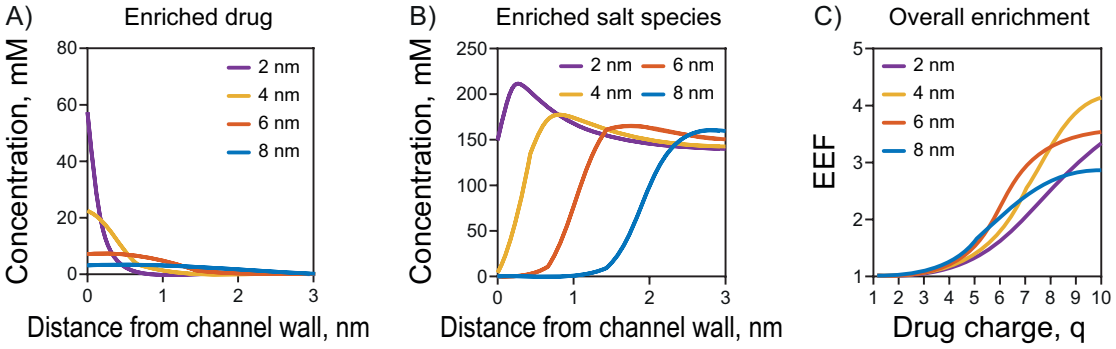

Figure 4.8: Simulations performed in a 1xPBS solution with a pH value equal to 7. Drug bulk concentration is 0.1 mM. Drug diameters from 2 nm to 8 nm are tested in all graphs. Other ionic species have a fixed dimension. A surface voltage of $-0.1\ V$ is applied. Concentrations curves of 10 q valence drug (**A**) and of Na^+ (**B**) are shown in the normal direction from the wall. **C**: overall EEF of drug in relationship with its valence.

which corresponds also to the obtaining of concentration saturation of drug as shown in figure 4.8.A and no more space is available for any ion next to Stern layer.

The overall effect of this phenomenon is that, when the drug is big enough to prevent the concentration of other counter-ions in the solution, and its maximum concentration is not achieved yet, the EEF of such a molecule increases with increasing its dimensions. Indeed, without other counter-ions species next to the wall, a higher mean concentration of drug is needed to screen the surface potential, leading to a higher enrichment factor.
This is exactly the result shown in figure 4.8.C where the different drug valences are related at respective EEF varying drug diameters. Increasing drug valence from 1 q to 10 q, a not linear increase of EEF is obtained for all curves at different diameters. But at maximum tested valence, the aforementioned phenomenon occurs and maximum enrichment factor is obtained for drug diameters equal to 4 nm. After this size value, EEF starts decreasing due to the even lower possible concentration caused by the increasing size of the molecule. This phenomenon has been called saturation mediated counter-ions exclusion because it results in the enrichment next to the channel wall of the most charged and not point-like ionic species in the solution and the consequent exclusion of other attracted ions with a finite volume due to the lack of space.

4.3.2 EEF saturation due to drug-salt ratio

In figures 4.9, 4.10, 4.12 and 4.13, the results obtained by the simulations of counter- and co-ions at different bulk concentrations, drug valences and salt concentrations are shown. Figures 4.9 and 4.12 show the relationship between drug valence and its EEF changing drug diameter from 2 nm to 8 nm. In this type of graphs drug reservoir concentration is set at 0.1 mM. Figures 4.10 and 4.13, rather, represent the EEF values associated with different bulk concentrations of drug in the reservoir, ranging drug valence from 2 q to 10 q. In these graphs the simulated drug has a ionic diameter equal to 1 nm.
For all figures below, first one of each group shows simulations performed in a 1xPBS solution, the second one in a 10%PBS solution, finally, the last one, in 1%PBS. Indeed the purpose of this analysis is to obtain results related with ionic strength of the solution and how this factor interacts with drug features listed before.

Counter-ions

Observing figure 4.9 it is possible to notice that an overall increase of EEF range takes place decreasing PBS percentage in the solution because the decrease of ionic strength results in a longer EDL.
Figure 4.9.A shows the simulations at 1xPBS, where the drug has a bulk concentration hundredfold less than salt and the maximum value for all curves is obtained at z_D=10 q. Differently, a completely not linearity of drug valence-EEF curves occurs in figures 4.9.B and 4.9.C. Indeed, it seems that not a higher enrichment value corresponds to higher drug charge, but the maximum value is reached at z_D=6

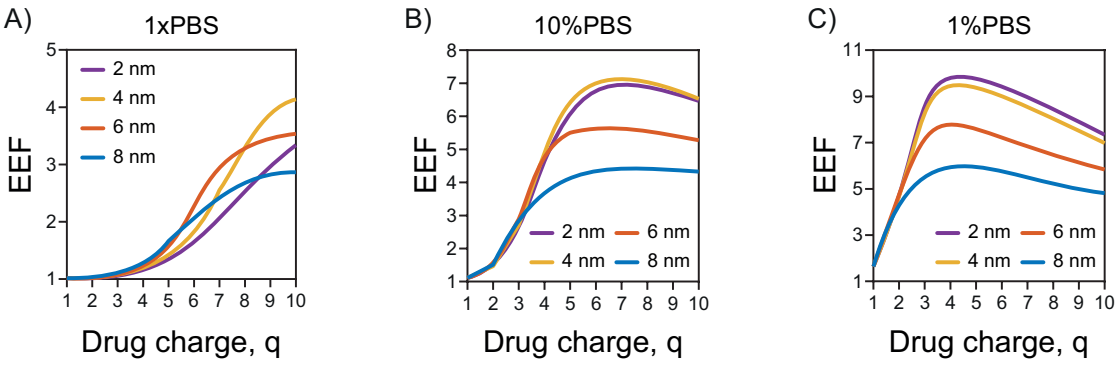

Figure 4.9: EEF of counter-ion drug in relationship with its valence at different ionic diameters. Its bulk concentration in the reservoir is 0.1 mM. Applied surface voltage is $-0.1\ V$. Simulations are performed in a 1xPBS (**A**), 10%PBS (**B**) and 1%PBS (**C**) solution.

q for tests at 10%PBS. After this maximum value, the EEF decreases increasing molecule valence. Instead, for tests performed at 1%PBS the maximum value is reached at z_D=4 q.

This phenomenon can be motivated observing figure 4.10. Indeed, as highlighted by vertical red dashed lines that represent the respective salt concentrations used in the parametric simulations, the ratio between drug and salt concentrations has a main role on EEF.
Taking as example figure 4.10.C, EEF at drug bulk concentration equal to 1 μM seems being linearly related with drug valence, even if already at this low drug concentration, enrichment values of drug with charge higher than 5 q are similar. However, if drug concentration increases, it is clear that highest valences molecules become more and more the less enriched species. Furthermore, if figure 4.10.A is analyzed, where all tested drug concentrations from 1 μM to 100 mM have a drug-salt ratio minor than 1, for almost all concentrations the most charged drug achieves the highest enrichment.
This analysis suggests that the compensation of drug by salt ions Na^+ or Cl^- (tables 2.2 and 2.4), caused by the assumption of a not-zero charge of the drug once it is dissolved inside the electrolyte solution, leads to an excessive amount of salt ions in the solution that is not related with initial PBS percentage but it is only dependant from drug bulk concentration. This case takes place when the drug-salt ratio is slightly less or more than 1. Indeed, in these conditions drug properties as its valence induce a compensation by salt ions that increases the ionic strength of solution as more as drug charge is high. For this reason in figures 4.9.B and 4.9.C, where drug-salt ratio is next to 1, the presence of a high valence drug causes an excessive dispersion of salt ions in the solution increasing its ionic strength and

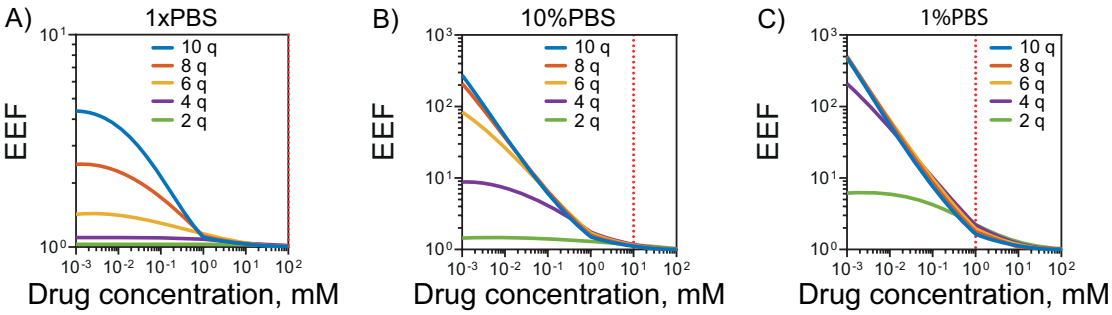

Figure 4.10: EEF of counter-ion drug in relationship with its concentration in the reservoir at different valences. Its tested diameter is 1 nm. Applied surface voltage is $-0.1\ V$. Simulations are performed in a 1xPBS (**A**), 10%PBS (**B**) and 1%PBS (**C**) solution as highlighted by red dashed lines.

consequently decreasing EDL length and its effect, producing an overall reduction of EEF values.

Once the relation between drug charge and respective enrichment is analyzed, now the influence of its ionic diameter is focused.
Observing figure 4.9 different behaviors can be recognized. In figure 4.9.C, where the enrichment factors achieve a high range of values, due to the low ionic strength of solution, a high ionic diameter leads to a general lower enrichment of the drug next to the wall due to the saturation of its concentration. Indeed, with diameter equal to 8 nm and considering ions as cubes whose side is their diameter, the maximum possible concentration is around 3.24 mM. The other maximum values are shown in figure 4.11. The effect of saturation becomes more relevant at highest enrichment conditions as it is possible to observe at respective drug valences which correspond to maximum EEF.

Nevertheless, it is already possible to notice the phenomenon of saturation mediated counter-ions exclusion in figure 4.9.B that becomes relevant in figure 4.9.A: the maximum enrichment curve does not correspond to lower ionic diameter. For this reason, a larger ionic diameter leads to lower mean concentration of the drug only if the enrichment is sufficiently high to achieve its saturation, if not, its EEF will rather be higher than a smaller drug.

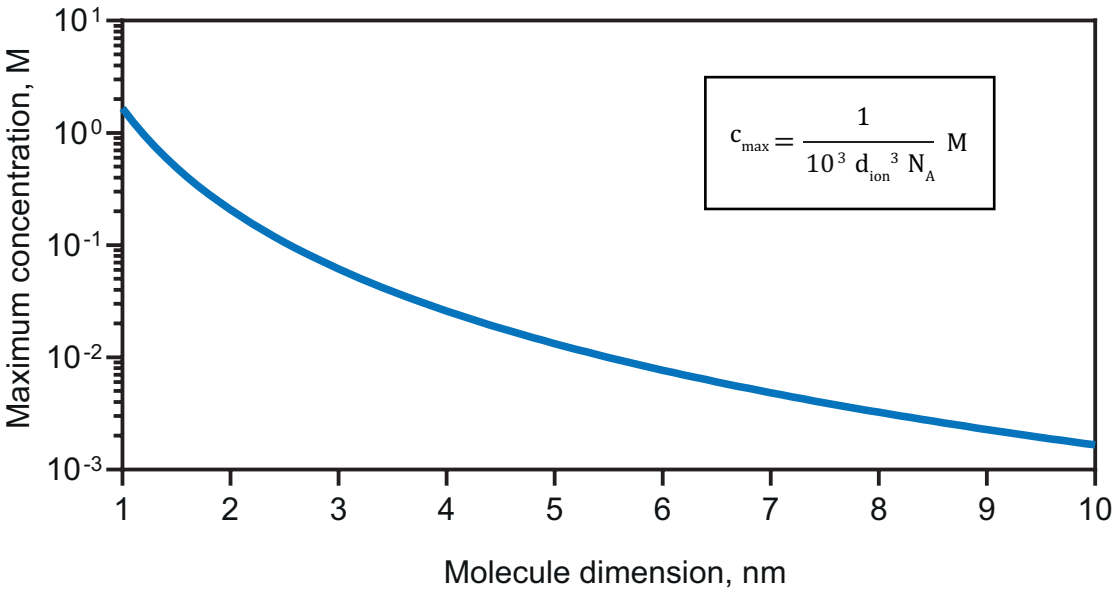

Figure 4.11: Maximum possible concentrations at respective ionic diameters of counter-ion drug considered with a cubic shape

It is generically clear from figure 4.10 that diffusive flux of drug, represented by its mean concentration in the channel, is not enhanced by the increase of its concentration in the reservoir. The presence of a higher amount of drug on one side of the membrane does not lead to an increased diffusive flux and a higher EEF value. This behavior was already foreseen due to the known fact that a nanochannel membrane leads to an effective independence of diffusive flux from bulk concentration in the reservoir [3].

Co-ions

The effects of drug compensation by salt ions can be recognized in figure 4.12.C, even if they are less important than counter-ions. At this salt concentration and only at highest tested drug valences, curves start increasing their EEF values.
Indeed, as shown in figures 4.12.A and 4.12.B, the relation between drug valence and respective depletion is almost linear already in 10%PBS solution.
Analyzing figure 4.13, the compensation by salt ions assumes a main role when drug-salt ratio is bigger or equal than 1, and in these cases a higher valence causes a minor depletion. But for co-ions this behavior does not occur already at ratios just less than 1, as for counter-ions.
Generically, co-ions drug, when their concentration is sufficiently lower than salt ones, present a more linear relationship between their valence and EEF than counter-ions. This aspect could be really useful when a new drug is tested due to the easier exclusion forecasting if it is meant to be used as a co-ion.

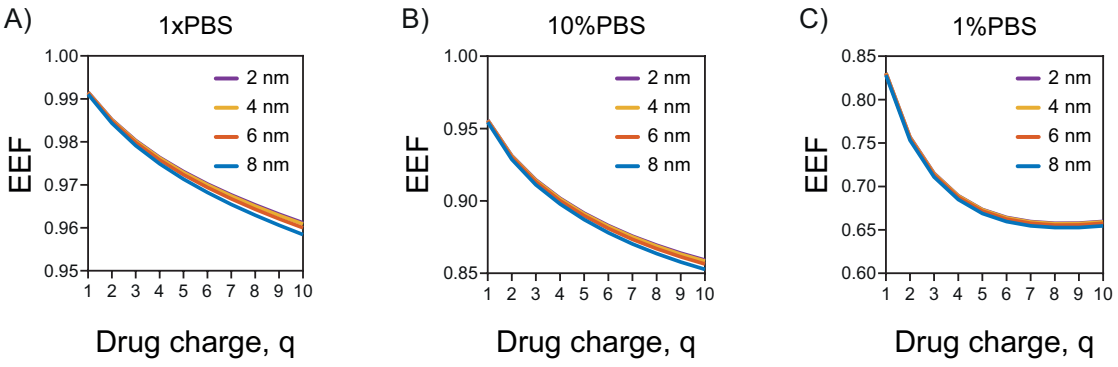

Figure 4.12: EEF of co-ion drug in relationship with its valence at different ionic diameters. Its bulk concentration in the reservoir is 0.1 mM. Applied surface voltage is 0.1 V. Simulations are performed in a 1xPBS (**A**), 10%PBS (**B**) and 1%PBS (**C**) solution.

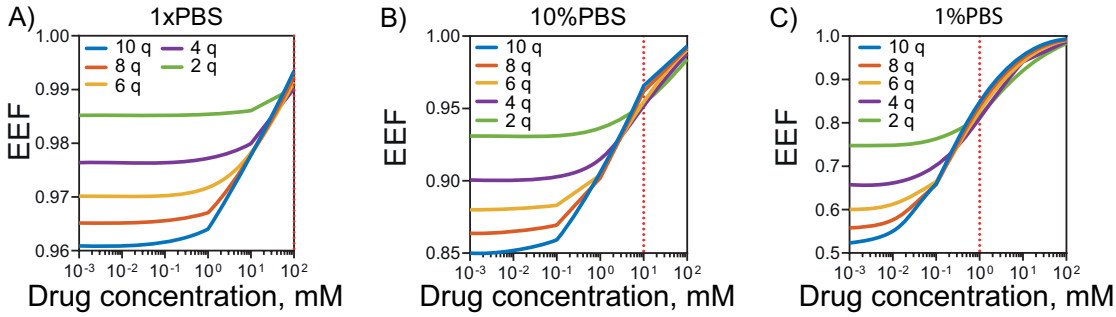

Figure 4.13: EEF of co-ion drug in relationship with its concentration in the reservoir at different valences. Its tested diameter is 1 nm. Applied surface voltage is 0.1 V. Simulations are performed in a 1xPBS (**A**), 10%PBS (**B**) and 1%PBS (**C**) solution as highlighted by red dashed lines.

If for counter-ions the relevance of molecule size assumes a not negligible role, it is marginal for co-ions, as it shown in figure 4.12. Obviously, the saturation of molecules cannot take place for this ionic species, so there are not important differences between large and small molecules when they are depleted, especially when the channel used in the simulation is 150 nm high, excluding from single-file diffusion case [13]. This particular instance happens when the dimension of channel forces the exclusion of molecules due to their size because they cannot geometrically enter inside the channel, or they are forced to create a single line of molecules that passes through it.
This FE model has not the purpose of studying this specific case. Indeed, in a biomedical application for a drug controlled release, the case of such a poor molecules flux caused by channel dimensions makes this device useless for an efficient medical treatment.

Chapter 5

Comparison with experimental data

5.1 Introduction

One of the most important task of this thesis was to rightly simulate experimental results obtained by Dr. Grattoni's laboratory at Houston Methodist Research Institute with nanofluidic membranes developed by Dr. Grattoni and Di Trani [10]. These membranes were negatively electrostatically gated to obtain a tunable control on different species of negatively charged drugs. These membranes show an incredible effectiveness on stopping the drugs diffusion in front of an efficacious amount of medication for patient treatment when no external voltage is applied to the membrane, thanks to the large height of channels, around 300 nm, that allows the diffusion of a sufficiently high quantity of molecules during passive phases [10, 11].
These membranes were manufactured to obtain 300 nm width channels, where solution is in contact with 60 nm of silicon carbide, which is used as dielectric material between electrolytic solution and Poly-Silicon buried electrode. Their structure was previously shown in figure 1.3.
In figure 5.1 the results obtained by Di Trani are shown. In figure 5.1a and 5.1c negative drugs had been diluted in a slightly low concentrated solution. Indeed, a 1%PBS solution was used to perform these tests. For this reason, as aforementioned in table 1.1, the effectiveness of EDL on drug diffusion is much higher than that results from the tests performed in 1xPBS solution and shown in figure 5.1b.
The results of drug release shown in figure 5.1 are represented as percentage of the value obtained at passive phase.
The application of a gate voltage immediately leaded to an impressive drop that at highest voltages (3V in figure 5.1a) almost stopped the drug release.

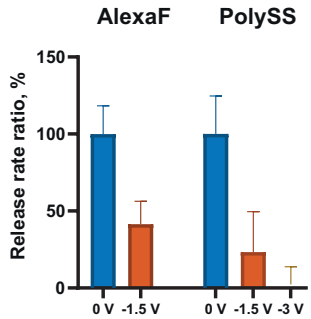

(a) Tests with Alexa Fluor and PolySS, which have a negative charge of -3q and -380q respectively, both tests occurred in 1%PBS solutions [10]

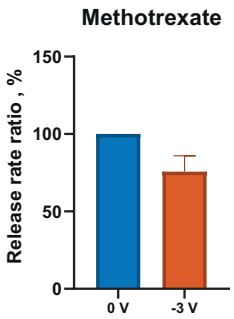

(b) Tests with Methotrexate, which has a negative charge of -2q, test occurred in 1xPBS solution [11]

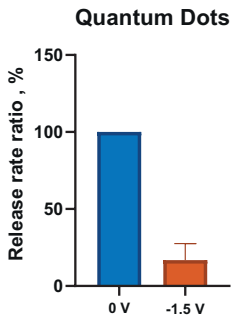

(c) Tests with quantum dots, which have a negative charge around -5 and -15q, test occurred in 1%PBS solution [11]

Figure 5.1: Experimental results of normalized release rates compared with passive phases performed by Dr. Grattoni and Di Trani with 300 nm width nanochannel membrane at different negative gate voltages [10, 11].

The membrane also shows a tunable behavior due to the fact that modulation of applied voltages results in a differentiation of release rates as well.
These results represent an incredible goal for controlled drug release applications. Indeed, with a not incredibly high voltage, which prevents from a too high power consumption, it has been possible to stop the release of a drug and, with the same device, to obtain a sufficient release in passive phases for an effective medical treatment.

5.2 FEM application

The purpose of this FE model was to obtain a sufficiently realistic model to simulate the nanofluidic membrane behavior. Indeed, for such a high channel width, results much less impressive were expected. So, it is hypothesized that SiC layer inside the channel presents a higher porosity than expected, behaving not as an ideal 60nm-thick dielectric.

5.2.1 Nanofluidic membrane parameters

Due to the different materials used in studied membrane, some changes have to be done to previously used parameters.

First of all, as aforementioned, to simulated the membrane, silicon carbide is used as dielectric material, having an relative electrical permittivity equal to 9.7.

Then, the Stern capacitance previously used is changed to be adapted to the new tests. The previous value of 0.3 F/m^2 used for distributed Stern layer capacitance, is six-fold increased to 1.8 F/m^2. This assumption is based on the experimentally measured values of capacitance at solid-liquid interface performed with silicon carbide [11].

The tested channel height is 300 nm, value experimentally measured by Di Trani [10]. One of the most puzzling parameter is the dielectric layer thickness. Indeed, due to the vapour deposition technique used, it is possible that dielectric layer deposition had created a 60nm-thick film with higher porosity than on external surface, which could cause a not ideal functioning. It is hypothesized that dielectric layer acts as a much thinner ideal SiC one, because the control on charged drug with a not excessive gate voltage is extremely high. Indeed, nanochannels array is vertically aligned compared to external membrane surface, which means that the deposition of silicon carbide could be not extremely accurate. For this reason the dielectric thickness is changed to 1 nm to evaluate this hypothesis.

Finally, silicon carbide is much less reactive than silicon dioxide causing a surface charge density which is around -0.2 $\mu C/m^2$ [10]. As initially tested during model development and as supposed by Kim in his study on a chemically treated surfaces which shows that a more than 10-fold reduction of silicon dioxide charge can be simulated as a not reactive material [13], all the comparison tests with experimental results are performed assuming a zero surface charge density.

5.2.2 FEM results compared with experimental data

In figure 5.2 the simulations results are compared with experimental data previously mentioned. On vertical axes the exclusion/enrichment factors (EEF) are represented as percentage values. Both curves about simulations using 1 nm and 60 nm as silicon carbide thickness are shown.

The realism of the model is evaluated with three different probes: the mean concentration of drug in the overall channel in the bi-dimensional model (EEF 2D) normalized with passive phase value, the ratio between diffusive fluxes of drug in active and passive phases through the channel calculated by the bi-dimensional model (Drug flux) and the mean concentration of drug calculated by the single-dimensional FE model initially described (EEF 1D).

All model results are normalized with passive phase EEF values, which simulate a normal diffusion between reservoir and sink of the drug due to the absence of any electric potential, externally applied or naturally shown by the silicon carbide surface.

As generally shown in figure 5.2, the comparison between different silicon carbide thicknesses supports the assumption that the dielectric layer inside the channels does not behaves as an ideal 60 nm thick film, but as a much thinner one. Results obtained with 60 nm thick dielectric layer from bi-dimensional model poorly reproduce experimental ones, differently from those obtained with 1 nm thick dielectric.

The results obtained from single dimensional model do not fit correctly experimental tests as well. Indeed, also at minor dielectric thickness value, EEF, calculated as the ratio between mean concentration of drug along normal direction from wall and bulk concentration, does not considerably decrease as the applied gate voltage. These different results from single and bi-dimensional models can be explained by the not consideration of the diffusion of a charged species between the reservoir and the sink. Indeed, Donnan equilibrium phenomenon previously described causes an electric potential gradient axially to the nanochannel. This potential leads to a not zero electric field in the middle of channel that affects ions concentrations also in the case of a not overlapped EDL. This case is impossible to evaluate in a single dimensional model.
Therefore, results obtained from 2D FEM are considered more trustworthy than those obtained by a 1D model that does not consider the diffusion effects.

Results obtained from drug flux probes are slightly different from those calculated as the mean concentration in the 2D channel, but still follow the same trend.

It demonstrates that the assumption based on literature that EEF calculated as the ratio between mean concentrations in the channel in active and passive phases can be considered as representative of effective permeability and the ratio between drug fluxes in the two cases.

For these reasons, the EEF values calculated as the normalized mean concentration in 2D model are considered the most reliable results obtained in the simulations with 1 nm thick silicon carbide layer. Therefore, here below are listed the exact values of experimental results and of FE model obtained from EEF 2D probe with the thinnest dielectric layer.

Alexa Fluor, shown in figure 5.2.A is set in the reservoir with a bulk concentration equal to 0.26 mM, its charge is -3 q and its ionic diameter is 1 nm. The simulation is performed at 1%PBS and two gate voltages are used: 0 V (passive phase) and -1.5 V (active phase).
At gate voltage equal to -1.5 V, the experimental reduction of this drug has been measured as almost 60% [10], the model has simulated a reduction of 40%.

It was impossible to perform an entire simulation on a drug identical to poly(sodium 4-styrenesulfonate) or PolySS, due to its excessive charge of -380q. For this reason, its simulation is performed with a relatively less charged drug, but still with a high valence compared to others. Indeed, -15 q is chosen as representative charge for PolySS, its concentration at reservoir is 2.8 μM and its ionic diameter is set as 5 nm. Here, three different states are defined: passive phase ($V_g = 0\ V$) and two active phases at -1.5 V and -3 V.
The results are shown in figure 5.2.B, the membrane has obtained a reduction of 77% and almost 100% for gate voltages equal to -1.5 V and -3 V, respectively [10]. FE model has obtained as results for same V_g values, 88% and 99.5% respectively. These results are extremely close to experimental ones. The simulation is again performed in a 1%PBS solution.

In figure 5.2.C the results obtained simulating methotrexate are shown. Its valence, ionic diameter and bulk concentration are set -2 q, 1.5 nm and 5.506 mM, respectively. The simulation is performed in a 1xPBS solution. Indeed, EE factors both experimentally and with model are the highest obtained in all tests even if, in the unique active phase, used gate voltage is -3 V.
Due to the reduced EDL extension inside the nanochannel caused by the higher ionic strength of the solution, the effect of electrostatic gating is less influential. The experimental tests have obtained as result a mean reduction in active phase ($V_g = -3\ V$) equal to 24% [11], FE simulation has proposed a reduction of 12%.

Finally, tests using quantum dots as drug are shown in figure 5.2.D. The tests are performed with a passive and an active phase, with 0 V and -1.5 V as gate voltages, respectively. Due to the variable range of charge proposed above (from -5 q to -15 q), the mean value of -10 q is chosen in the *in silico* simulation. The values of 5 nm and 5 μM are set as ionic diameter and bulk concentration in the reservoir, respectively. The solution concentration is maintained to 1%PBS.
Experimental reduction in active phase is equal to 84% and the FE model has presented a value of 78% [11].

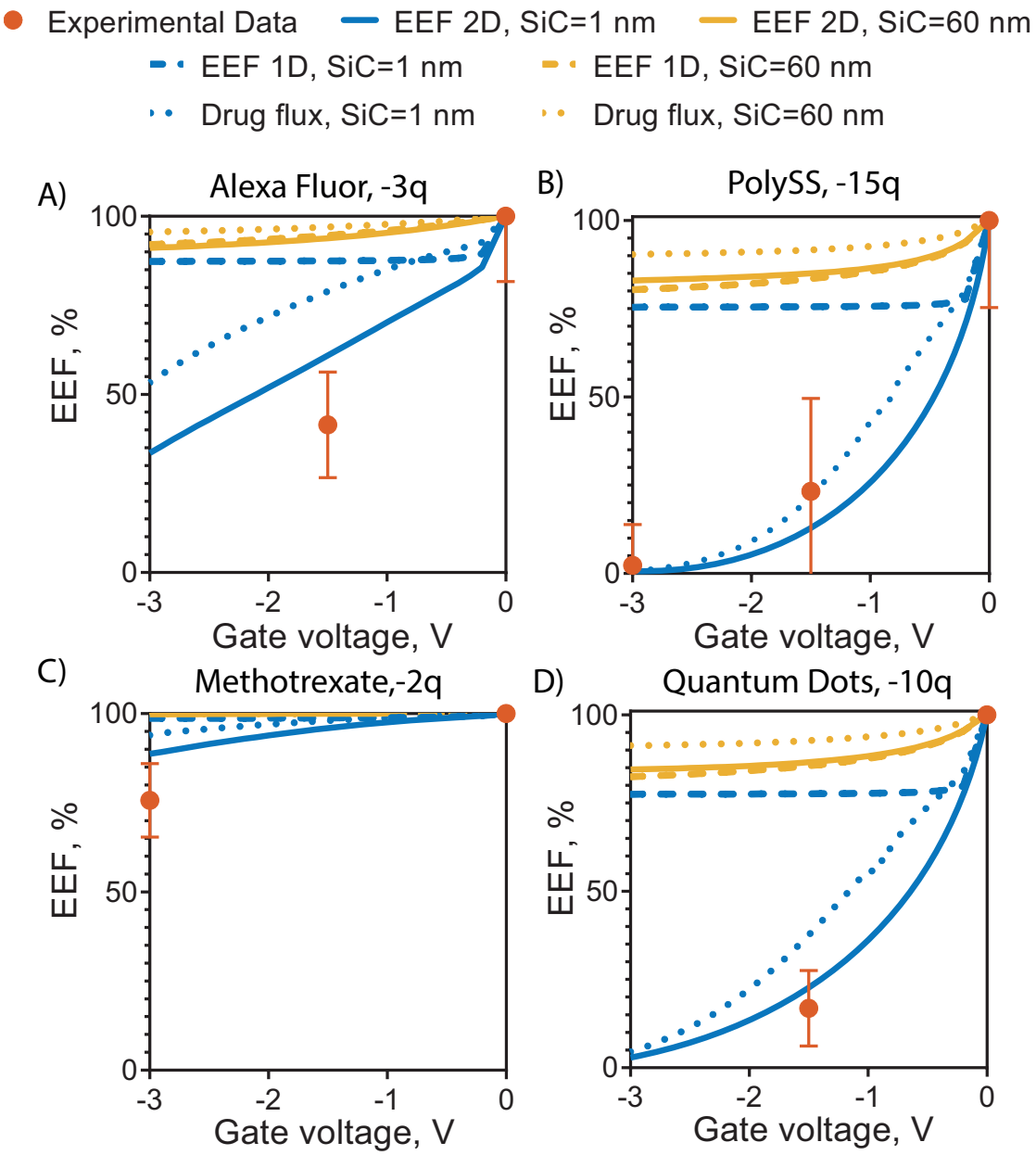

Figure 5.2: Model results obtained reproducing nanofluidic membrane experimental tests. Different silicon carbide layer thicknesses are tested. The shown results are obtained from different probes and models. **A**: Alexa Fluor, -3q charge, diluted in 1%PBS solution; **B**: a high valence drug (-15q), reproducing PolySS drug, diluted in 1%PBS solution; **C**: Methotrexate, -2q charge, diluted in 1xPBS solution; **D**: Quantum Dots, -10q assumed charge, diluted in 1%PBS solution. The concentrations of each drug is 0.26 mM, 2.8 μM, 5.506 mM and 5 μM, respectively. In the same way, the ionic diameters assigned to each drug molecule are 1 nm, 5 nm, 1.5 nm and 5 nm, respectively.

Chapter 6

Conclusion

The model has demonstrated the influence of different parameters as ionic strength of the solution, its pH value, channel dimension and its manufacturing properties (dielectric material type and its thickness) on the diffusion of a charged molecule through a gated nanochannel.
Externally applied electric potential has been demonstrated to be a relevant parameter and its effects on drug flux can be considered as regular and predictable, which is a useful behavior in a controlled drug delivery application.
Drug properties as its charge, its bulk concentration and its dimension have been tested and obtained results have demonstrated that all these parameters cause related effects on exclusion or enrichment of ions.
Indeed, it has been demonstrated that a low ionic strength of solution causes a high range of EEF values for counter-ion drug, but its linearity with its valence decreases. Nevertheless, in these cases, saturation of counter-ions establishes a inversely linear relationship between enrichment and ionic dimensions.
On the other hand, when a higher ionic strength of the solution leads to lower EEF values, the relationship between drug valence and its enrichment becomes more linear but these conditions introduce the unexpected saturation mediated counter-ions exclusion phenomenon. The exclusion of other counter-ions species from charged wall due to the excessive volume of the most enriched ions (the drug in this case) causes a not linear relationship between drug enrichment and its diameter.
Co-ion drug species results having an overall higher independence on their ionic diameters and drug-salt ratio. For this reason, in a drug delivery application, where the same membrane can be used for different types of drug, with variable dimensions and bulk concentrations, the choice of using co-ion drugs against counter-ion type due to their more predictable behaviors is rightful.

The developed model has rightly simulated the experimental results obtained

by the nanofluidic membranes tested by Alessandro Grattoni and Nicola Di Trani at Houston Methodist Research Institute. The finite element simulations have supported the hypothesis that a not ideal dielectric layer of silicon carbide is present inside the nanochannels and due to the high porosity of this material, confirmed also by its higher capacitance than SiO_2, its behavior can be reproduced as a much thinner ideal layer.
Thanks to the comparison from these data, the developed FE model demonstrates that the use of a bi-dimensional, at least, model is necessary to obtain a sufficiently high fit of realistic data.
Starting from previous FEMs presented in literature, the model developed in this thesis achieves a higher realism introducing a finite-size modified Poisson-Nernst-Planck equation. This type of equations was implemented only in numerical models that do not consider the complete bi-dimensional geometry of the system. In this FEM these two aspects are combined to obtain an achieved better fit with experimental data. For these reasons, the assumption of the need of a complete model that simulates both phenomena, exclusion/enrichment due to the EDL and diffusion of a diluted charged molecule, must be considered.

Bibliography

[1] RameshBabu Chandran. «Finite Element Analysis in Nanotechnology Research». In: (November 2020). URL: DOI:%20http://dx.doi.org/10.5772/intechopen.94590 (cit. on pp. 2, 4).

[2] Carl H. Hamann, A. Hamnett, and Wolf Vielstich. *Electrochemistry*. 2. completely revised and updated ed. Weinheim: Wiley-VCH, 2007. ISBN: 9783527310692 (cit. on p. 2).

[3] Alessandro Grattoni et al. «Gated and near-surface diffusion of charged fullerenes in nanochannels». In: *ACS nano* 5.12 (2011), pp. 9382–9391. DOI: 10.1021/nn2037863 (cit. on pp. 2, 51).

[4] A. Ziemys, A. Grattoni, D. Fine, F. Hussain, and M. Ferrari. «Confinement effects on monosaccharide transport in nanochannels». In: *The journal of physical chemistry. B* 114.34 (2010), pp. 11117–11126. DOI: 10.1021/jp103519d (cit. on p. 2).

[5] Frank H. J. van der Heyden, Derek Stein, and Cees Dekker. «Streaming currents in a single nanofluidic channel». In: *Physical review letters* 95.11 (2005), p. 116104. ISSN: 0031-9007. DOI: 10.1103/PhysRevLett.95.116104 (cit. on p. 2).

[6] W. Sparreboom, A. van den Berg, and J. C. T. Eijkel. «Principles and applications of nanofluidic transport». In: *Nature nanotechnology* 4.11 (2009), pp. 713–720. DOI: 10.1038/nnano.2009.332 (cit. on p. 2).

[7] G. Pardon and W. van der Wijngaart. «Modeling and simulation of electrostatically gated nanochannels». In: *Advances in colloid and interface science* 199-200 (2013), pp. 78–94. DOI: 10.1016/j.cis.2013.06.006 (cit. on pp. 2, 4, 6, 8, 10, 14, 16, 20, 26–28).

[8] Weihua Guan, Sylvia Xin Li, and Mark A. Reed. «Voltage gated ion and molecule transport in engineered nanochannels: theory, fabrication and applications». In: *Nanotechnology* 25.12 (2014), p. 122001. DOI: 10.1088/0957-4484/25/12/122001 (cit. on pp. 2, 6).

[9] Reto B. Schoch, Jongyoon Han, and Philippe Renaud. «Transport phenomena in nanofluidics». In: *Reviews of Modern Physics* 80.3 (2008), pp. 839–883. ISSN: 0034-6861. DOI: 10.1103/RevModPhys.80.839 (cit. on pp. 3–5, 31, 32, 42).

[10] Nicola Di Trani, Antonia Silvestri, Antons Sizovs, Yu Wang, Donald R. Erm, Danilo Demarchi, Xuewu Liu, and Alessandro Grattoni. «Electrostatically gated nanofluidic membrane for ultra-low power controlled drug delivery». In: *Lab on a chip* 20.9 (2020), pp. 1562–1576. DOI: 10.1039/d0lc00121j (cit. on pp. 4, 5, 7, 14, 41, 53–55, 57).

[11] Nicola Di Trani, Antonia Silvestri, Yu Wang, Danilo Demarchi, Xuewu Liu, and Alessandro Grattoni. «Silicon Nanofluidic Membrane for Electrostatic Control of Drugs and Analytes Elution». In: *Pharmaceutics* 12.7 (2020). ISSN: 1999-4923. DOI: 10.3390/pharmaceutics12070679 (cit. on pp. 4, 44, 53–55, 57, 58).

[12] Adrien Plecis, Reto B. Schoch, and Philippe Renaud. «Ionic transport phenomena in nanofluidics: experimental and theoretical study of the exclusion-enrichment effect on a chip». In: *Nano letters* 5.6 (2005), pp. 1147–1155. ISSN: 1530-6984. DOI: 10.1021/nl050265h (cit. on p. 5).

[13] Sungho Kim, Ece Isenbike Ozalp, Vignesh Sundar, Jian-Gang Zhu, and Jeffrey A. Weldon. «Modeling of electrically controlled molecular diffusion in a nanofluidic channel». In: *Journal of Applied Physics* 118.7 (2015), p. 074301. ISSN: 0021-8979. DOI: 10.1063/1.4928607 (cit. on pp. 5, 8, 17, 52, 55).

[14] Nicola Di Trani, Alberto Pimpinelli, and Alessandro Grattoni. «Finite-Size Charged Species Diffusion and pH Change in Nanochannels». In: *ACS applied materials & interfaces* 12.10 (2020), pp. 12246–12255. DOI: 10.1021/acsami.9b19182 (cit. on pp. 5, 11).

[15] A. Eden, C. McCallum, B. D. Storey, S. Pennathur, and C. D. Meinhart. «Analyte preconcentration in nanofluidic channels with nonuniform zeta potential». In: *Physical Review Fluids* 2.12 (2017). DOI: 10.1103/PhysRevFluids.2.124203 (cit. on p. 8).

[16] Sungho Kim, Ece Isenbike Ozalp, Mohamed Darwish, and Jeffrey A. Weldon. «Electrically gated nanoporous membranes for smart molecular flow control». In: *Nanoscale* 10.44 (2018), pp. 20740–20747. DOI: 10.1039/c8nr05906c (cit. on pp. 8, 41).

[17] Zhijun Jiang and Derek Stein. «Electrofluidic gating of a chemically reactive surface». In: *Langmuir : the ACS journal of surfaces and colloids* 26.11 (2010), pp. 8161–8173. DOI: 10.1021/la9044682 (cit. on pp. 14, 15, 27).

[18] T Hiemstra, J.C.M De Wit, and W.H Van Riemsdijk. «Multisite proton adsorption modeling at the solid/solution interface of (hydr)oxides: A new approach: II. Application to various important (hydr)oxides». In: *Journal of Colloid and Interface Science* 133.1 (1989), pp. 105–117. ISSN: 0021-9797. DOI: 10.1016/0021-9797(89)90285-3. URL: https://www.sciencedirect.com/science/article/pii/0021979789902853 (cit. on p. 14).

[19] M. Taghipoor, A. Bertsch, and Ph Renaud. «An improved model for predicting electrical conductance in nanochannels». In: *Physical chemistry chemical physics : PCCP* 17.6 (2015), pp. 4160–4167. DOI: 10.1039/c4cp05338a (cit. on pp. 14, 15, 27).

[20] Rohit Karnik, Rong Fan, Min Yue, Deyu Li, Peidong Yang, and Arun Majumdar. «Electrostatic control of ions and molecules in nanofluidic transistors». In: *Nano letters* 5.5 (2005), pp. 943–948. ISSN: 1530-6984. DOI: 10.1021/nl050493b (cit. on p. 14).

[21] David E. Yates, Samuel Levine, and Thomas W. Healy. «Site-binding model of the electrical double layer at the oxide/water interface». In: *Journal of the Chemical Society, Faraday Transactions 1: Physical Chemistry in Condensed Phases* 70.0 (1974), p. 1807. ISSN: 0300-9599. DOI: 10.1039/f19747001807 (cit. on p. 14).

[22] Weihua Guan, Rong Fan, and Mark A. Reed. «Field-effect reconfigurable nanofluidic ionic diodes». In: *Nature communications* 2 (2011), p. 506. DOI: 10.1038/ncomms1514 (cit. on pp. 16, 17).

[23] Christopher Hughes, Li-Hsien Yeh, and Shizhi Qian. «Field Effect Modulation of Surface Charge Property and Electroosmotic Flow in a Nanochannel: Stern Layer Effect». In: *The Journal of Physical Chemistry C* 117.18 (2013), pp. 9322–9331. ISSN: 1932-7447. DOI: 10.1021/jp402018u (cit. on pp. 18, 21, 44).

[24] N. S. Bolan and K. Kandaswamy. «pH». In: *Encyclopedia of Soils in the Environment*. Ed. by Daniel Hillel. Oxford: Elsevier, 2005, pp. 196–202. ISBN: 978-0-12-348530-4. DOI: 10.1016/B0-12-348530-4/00210-1. URL: https://www.sciencedirect.com/science/article/pii/B0123485304002101 (cit. on p. 20).

[25] P.W. Atkins. *Physical Chemistry*. 5th. 1994. ISBN: 0-19-855731-0 (cit. on p. 20).

[26] Martin Z. Bazant, Mustafa Sabri Kilic, Brian D. Storey, and Armand Ajdari. «Towards an understanding of induced-charge electrokinetics at large applied voltages in concentrated solutions». In: *Advances in colloid and interface science* 152.1-2 (2009), pp. 48–88. DOI: 10.1016/j.cis.2009.10.001 (cit. on p. 33).

[27] Achraf Ben Amar, Ammar B. Kouki, and Hung Cao. «Power Approaches for Implantable Medical Devices». In: *Sensors (Basel, Switzerland)* 15.11 (2015), pp. 28889–28914. DOI: 10.3390/s151128889 (cit. on p. 40).

[28] Yoon Kyeung Lee et al. «Dissolution of Monocrystalline Silicon Nanomembranes and Their Use as Encapsulation Layers and Electrical Interfaces in Water-Soluble Electronics». In: *ACS nano* 11.12 (2017), pp. 12562–12572. DOI: 10.1021/acsnano.7b06697 (cit. on p. 41).

[29] Alessandro Grattoni et al. «Nanochannel technology for constant delivery of chemotherapeutics: beyond metronomic administration». In: *Pharmaceutical research* 28.2 (2011), pp. 292–300. DOI: 10.1007/s11095-010-0195-6 (cit. on p. 41).

Ringraziamenti

Premetto che non mi ricorderò di nominare tutte le persone a cui vorrei rivolgere i miei ringraziamenti, a questi porgo le mie scuse e sappiano che comunque hanno un posto nel mio cuore.

Un enorme e sentito ringraziamento va al Dr. Alessandro Grattoni e allo Houston Methodist Research Institute per avermi concesso l'occasione di svolgere questa tesi. É stato per me un onore lavorare al progetto da loro portato avanti di un dispositivo impiantabile attivo per il rilascio controllato di farmaco, è stato ispirante sia dal punto di vista umano che lavorativo. Se ripenso al giorno in cui tre anni fa il professor Grattoni venne a tenere una lezione al Politecnico concludendo con "...per chiunque fosse interessato e altamente motivato, sappiate che c'è la possibilità di svolgere con noi la tesi...", seguito da un mio classico "Ma figurati se...", mi sembra passata una vita.

Un grazie in particolare va al mio fantastico correlatore Nicola Di Trani, per l'estrema disponibilità sempre dimostratami e per l'enorme aiuto che mi ha fornito per svolgere questo lavoro. Lavorare con lui è stata un'esperienza che mi ha arricchito molto e che mi ha aiutato a fare chiarezza sulla mia futura carriera lavorativa. Le videochiamate con lui dalle 23.30 fino all'una di notte, spesso dopo due ore di allenamento saranno un ricordo che mi porterò sempre dentro ripensando a questa tesi. Spero un giorno ci potremo incontrare dal vivo e scoprire che non siamo solo volti su uno schermo.

Ringrazio il Politecnico di Torino, per la formazione accademica e non solo che mi ha fornito nell'arco di questi anni. Credo che la qualità di questo ateneo sia una delle migliori di cui ho avuto esperienza, e sarò sempre orgoglioro di essere stato parte di questa istittuzione. Un ringraziamento particolare va al mio relatore, il professor Danilo Demarchi, per la grande opportunità che mi ha concesso con questa tesi e per essere sempre stato disponibile ed avermi ogni volta parlato con calma e gentilezza, qualità che non sono scontate nel frenetico mondo universitario. Vorrei ringraziare inoltre tutto il corpo docenti, in particolare tutti i professori

che mi hanno avuto come alunno, questa tesi e quelle di tutti i miei colleghi è il risultato del loro lavoro e spero che ne siano fieri.

Ringrazio di cuore e con affetto tutti coloro che ho conosciuto durante i miei anni al Politecnico, che non sono stati solo colleghi, ma anche amici. Ringrazio in particolare Roberto Ruffinello, che non si sa come è riuscito a sopportarmi dal primo giorno di elementari fino all'ultimo giorno di università, con una breve pausa liceale. Sono quattordici anni che siamo compagni di classe, e ancora ti chiamo per chiederti quali sono i capitoli da studiare e i documenti da presentare, e tu sei sempre pronto ad aiutarmi, grazie! A Rosita, che è stata una cara amica per tutti gli anni di Politecnico, sempre presente, sempre sicera (ai limiti della sfacciataggine) e sempre pronta a farti passare le lezioni chiaccherando come due vecchiette. Grazie ad Andrea Zimara, che è sempre stato un grande collega ma soprattutto un grande amico fuori dalle lezioni, con un sorriso sempre pronto e una battuta per sollevarti di morale. Grazie ad Andrea Prestia, perchè è stato uno dei più motivanti amici e colleghi dell'università, che non chiedeva agli altri nè di più nè di meno di quanto potesse fare lui, spronandomi sempre a dare il massimo, spero che un giorno potremo essere colleghi. A Roberto Rivoli, detto Bobo, perchè è riuscito a farmi sorridere essendo semplicemente se stesso e facendomi sempre da spalla nella nobile arte di non fare assolutamente nulla di serio. Un grazie va a Luca Rabezzana. Nonostante le nostre carriere universitarie si siano divise, siamo sempre rimasti in contatto e mi dà sempre grande soddisfazione confrontarmi con lui, sono orgoglioso di conoscere un grandere lavoratore come lui e gli auguro il meglio per il futuro. Un ringraziamento con dal profondo del mio cuore va a tutti i colleghi ed amici che ho incontrato durante i miei anni universitari: Linda, Francesco Serrago (il Presidente), Alessandro e Luca Rapetti.

Ringrazio tutta la società del Cus Torino Rugby, ed in particolare la mia squadra, che è diventata negli anni la mia seconda famiglia. A loro devo molti momenti di gioia della mia vita ma anche di fatica, sudore, fango e botte, che comunque hanno sempre portato a grandi soddisfazioni. Con loro ho sperimentato negli anni cosa significhi sacrificarsi per qualcos'altro e qualcun altro. Mi hanno insegnato il valore del duro lavoro e della costanza, e anche di cosa significhi essere come una famiglia. Un ringraziamento particolare va a Lollo, con il quale ormai condivido la panchina in spogliatoio da anni e che ha sempre avuto il tempo di parlare con me su qualunque cosa e la cui conoscenza mi arricchisce ogni giorno di più. Grazie anche ad Alberto Dezzani, coinquilino per due anni della mia carriera universitaria, compagno di squadra e quasi fratello maggiore, grazie per tutto il tempo passato assieme, so che tu mi hai un po' cambiato, ma è vero anche il contrario, diciamocelo.

Grazie a Mauro, amico d'infanzia, praticamente di culla, a cui mi sono riavvicinato molto negli ultimi anni, e la cui opinione mi ha sempre aiutato. Egli è testimonianza per me che anche le amicizie più datate possono rinnovarsi ed assumere nuovi colori.

Grazie di cuore a tutte le persone conosciute durante il mio Erasmus a Tampere. É stata un'esperienza incredibile che mi ha fatto incontrare delle persone incredibili. Grazie al gruppo delle French Crepês, compagni di avventure ma anche intimo gruppo di amicizie, ognuna che portava qualcosa di speciale rendendo tutto più unico che mai. Grazie a tutti voi per le serate al karaoke urlando come degli idioti, per le regole della casa di Max, Francesco ed Ewen, per i viaggi che abbiamo fatto, per il cellulare di Fra in Lapponia, per il Mc Donald dell'una di notte e un'infinità di altri piccoli momenti di semplice felicità. Ringrazio Sophie, che mi è stata vicina durante questa esperienza che ha lasciato in entrambi un tenero ricordo. Ringrazio Carmen e Giovanni, non solo per tutto il tempo passato assieme in Finlandia, ma per essere rimasti presenti anche una volta tornati, la vostra compagnia accende sempre in me un barlume di gioia (soprattutto quando Carmen ti obbliga a giocare a 21 o Giovannino ti chiede "Do you want some watermelon?"). Ad Eleonora, la cui travolgente simpatia e socialità hanno reso l'Erasmus tra i banchi e fuori un'eperienza indimenticabile (confido di rivederci presto e che io possa finalmente verificare l'esistenza di Romans). A Francesco, perchè mi ha fatto ricredere sul poter essere così vicino ad una persona conoscendala da così poco, sei stato come un fratello per me in Finlandia e porterò sempre con me tutti i momenti passati assieme, le serate fino alle 5 di mattina nei locali con la peggior musica di Tampere per non pagare il pullman, il caffè con il Nazionale, le camminate di otto km dalla discoteca a casa alle 3 di notte in mezzo ai boschi, i beer pong nei sauna party, di tutto questo e di molto altro, ti ringrazio.

Ringrazio i miei amici del liceo, Franceschino, Giulia, Matteo e Cristina. Il liceo è dove ci siamo conosciuti, ma il nostro gruppo sicuramente non è finito lì. Grazie che ogni volta continuate a mostrarmi come si possa vivere la propria vita con leggerezza e che sempre basterà per essere felici un gruppo di care persone con cui sedersi e chiaccherare. Di questo e della sua grande pazienza ringrazio anche Bebe, che non ho nominato prima solo per farla arrabbiare, so che non mi perdonerai.

A Zappo, la cui amicizia negli anni si è evoluta in diversi modi e che sempre mi sorprende. Grazie a te so che non serve parlarsi per ore per essere vicini ma semplicemente codividere il tempo assieme, sia nei giorni in cui non vorresti parlare con nessuno che negli altri. Grazie per il costante esempio di forza di volontà che sei per me.

Grazie a Chiara, la mia più cara amica con cui potrei passare ore a parlare. Grazie per essere sempre stata una figura presente quando ne avevo bisogno, di avermi accolto dopo mesi che non ci vedevamo come se fosse passato solo qualche giorno. Grazie per essere la persona che sento più vicina a me anche quando ci separano migliaia di chilometri. Grazie per tutti i momenti passati assieme e per quelli che verranno. Ricorda che ci dobbiamo incontrare il 15 Agosto 2034.

Ad Alessio, il mio coinquilino in questi ultimi mesi di vita universitaria, per essere diventato in poco tempo un caro amico e che sempre ha saputo liberarmi dalle preoccupazioni con un sorriso e una Moretti da 66 stappata per me.

Un grazie di cuore a tutti i miei parenti, che mi hanno sempre sostenuto e motivato, insegnandomi cosa significhi volersi bene ed essere una famiglia.

Grazie a mio fratello Alessandro, perchè per me è motivo di orgoglio ed è diventato negli anni non solo un fratellone un po' scorbutico, ma anche un amico. Grazie del costante esempio che mi dai e di tutti i consigli che soprattutto in questi ultimi mesi di tesi mi sono stati tanto utili. Grazie per avermi sempre spronato a dare il meglio di me, credendo nelle mie capacità più di tutti, anche più di me. Grazie per essere sempre te stesso, senza compromessi e mostrarmelo ogni volta. Grazie fratellone.

A mia madre, grazie per essere semplicemente se stessa. Per avermi insegnato tutto quello che so e per aver fatto di me l'uomo che sono. Grazie per aver creduto in me per tutti questi anni ed avermi supportato. Grazie per avermi sempre dimostrato che non è il proprio lavoro che ti qualifica ma la passione che ci metti nel farlo. Grazie per essere stata paciere molte volte in situazioni di crisi e di esserti sobbarcata il peso di tenere unita la nostra famiglia anche senza che io ed Ale lo sapessimo. Grazie di questo e di un'infinità di altre cose che non potrei elencare tutte.

Grazie a mio padre, perchè è la mia colonna. Grazie per avermi insegnato cosa significa la forza di volontà e l'etica del lavoro. Grazie per essere sempre stato il mio riferimento come figura paterna e per avermi reso orgoglioso di essere tuo figlio. Grazie per non essere stato solo il padre intransigente ma anche una "madre" affettuosa, per saperti commuovere come un ragazzo a più di 60 anni e per accogliermi sempre con un abbraccio ed un bacio. Come ti dissi tempo fa, spero di diventare un giorno un padre come te.

Ad entrambi i miei genitori, questa tesi e tutto il mio percoso universitario, è dedicato a voi.